

*Chapter 3*

## ATMOSPHERIC INPUT OF MANGANESE AND IRON TO THE OCEAN:

## Seawater dissolution experiments with organic ligands

Jeffrey Mendez<sup>a</sup>, Kristen Buck<sup>b</sup>, Jess Adkins<sup>c</sup><sup>a</sup> Department of Environmental Science and Engineering, California Institute of Technology<sup>b</sup> Scripps Institute of Oceanography, University of California San Diego<sup>c</sup> Department of Geological and Planetary Sciences, California Institute of Technology*1. Introduction*

Iron (Fe) and Manganese (Mn) are essential elements to all biological organisms, including those of the marine environment. These micronutrients are required for enzymatic pathways of respiration, nitrogen and carbon fixation, and electron transfer in photosynthesis (Turner and Hunter, 2001). One of the largest sources of these metals to the oceans is atmospheric deposition (Duce and Tindale, 1991; Guieu *et al.*, 1994; Siefert *et al.*, 1998). Despite the fact that Fe and Mn are key to the ecology of the ocean, there is little mechanistic understanding of their dry aerosol dissolution.

Manganese within a fully oxygenated ocean at natural pH should be Mn(IV) and precipitate out of the water in the form MnO<sub>2</sub>. However, the surface ocean contains Mn(II) concentrations as high as 25 nM (Chapter 3). In the open ocean, a portion of this Mn(II) is the result of aerosol deposition (Guieu *et al.*, 1994). Much of the Mn contained within the dust is in the +2 oxidation state. Slow oxidation to the +3 or +4 state allows Mn to stay dissolved on the order of days (Stumm and Morgan, 1996); however, Mn should oxidize over time and precipitate out of the surface ocean. Accumulation of the oxidized Mn is prevented by continual photoreduction of Mn back to the +2 oxidation state by humic materials (Sunda *et al.*, 1983). This photoreduction prevents the Mn from

precipitating out of the surface ocean, and maintains sufficient concentrations of dissolved Mn for biological use.

Fe is the fourth most abundant element in the Earth's crust (Wedepohl, 1995), and yet its thermodynamically stable oxidation state, Fe (III), is relatively insoluble in oxic pH 8 seawater. This limits its inorganic concentration to 0.1 nM (Morel and Hering, 1993). Any inorganic iron above this concentration will either form an Fe oxide solid or quickly adsorb onto nearby surfaces (Rose and Waite, 2002). Despite this limit, oceanic Fe concentrations range from 0.1 – 2 nM (or higher in the coastal ocean, Chapter 3). Fe(II) additions to the surface water from wet or dry deposition can elevate the total dissolved Fe concentration (Erel et al., 1993; Johansen et al., 2000); however, these too will be quickly oxidized to Fe(III). Therefore, Fe must have a non-inorganic method for maintaining dissolved Fe in the seawater. Organic ligands appear to be responsible for this elevation of Fe concentrations. Specific Fe binding ligands called siderophores are produced by bacteria to acquire environmental Fe and strongly bind Fe(III) (Neilands, 1995). Some strong Fe binding ligands in the marine environment appear to resemble siderophores in functional group and molecular size (Macrellis *et al.*, 2001; Witter *et al.*, 2000), although these ligands have not yet been structurally identified (Rue and Bruland, 2001). Additionally, the siderophore aerobactin is produced by marine *Vibrio* bacteria grown under Fe limiting conditions (Haygood *et al.*, 1993). Aerobactin is a di-hydroxamate  $\alpha$ -hydroxy-carboxylate siderophore (Fig. 1), and its physical chemistry properties (Harris *et al.*, 1979) and cellular iron transport pathways are well characterized (Braun, 2003). In addition, large undifferentiated molecules, such as humic acids (Voelker *et al.*, 1997) as well as small organic molecules, may specifically facilitate Fe dissolution from dust into the ocean. Oxalate has been shown to dissolve Fe oxides in laboratory settings (Siffert and Sulzberger, 1991), while citrate has been shown to allow Fe concentrations above the inorganic threshold (Waite and Morel, 1984).

Ligand-controlled Fe oxide dissolution proceeds along three steps (Furrer and Stumm, 1986; Zinder *et al.*, 1986):

1. A fast surface complexation by the ligand in a ligand exchange mechanism,
2. A slow, rate-determining detachment of the Fe ion,
3. A fast regeneration of the surface and transport of the metal complex into the bulk solution.

In reductive dissolution, the second step of detachment is preceded by a ligand-to-metal charge transfer from either a thermally- or photolytically-excited ligand. The reduction of Fe polarizes and weakens the Fe-oxygen bonds in the mineral structure, which allows the slow detachment of Fe (Furrer and Stumm, 1986; Siffert and Sulzberger, 1991). This slow rate may lead to a competitive reoxidation of the Fe(II), resulting in even slower Fe dissolution. However, detachment of the Fe(II) from the surface occurs more rapidly in siderophore-promoted dissolution (Borer *et al.*, 2005). Due to its large negative redox potential, the Fe(II)-siderophore complex will quickly reoxidize to the more soluble and stable Fe(III)-siderophore complex once free of the original mineral surface (Boukhalfa and Crumbliss, 2002).

Many siderophores are highly photoreactive. While the hydroxamate moiety (*i.e.* desferrioxamine-B, DFOB) is photochemically inert in both the bound and unbound state (Barbeau *et al.*, 2003), photolysis of the Fe(III)- $\alpha$ -hydroxy carboxylate siderophore (*i.e.* Fe-aerobactin) complex leads to a ligand-to-metal charge transfer and reduction of Fe(III) to Fe(II) (Barbeau *et al.*, 2001; Barbeau *et al.*, 2002). This results in cleavage of small functional groups and decarboxylation of the ligand. In addition, the ligand photo-product can retain strong Fe binding capability from enolate sites formed during decarboxylation (Küpper *et al.*, 2006).

We previously investigated the dissolution of Fe and Mn (Mendez *et al.*, in review) and found that Mn dissolution was proportional to dust concentration. Fe dissolution was found to not only be independent of dust concentration, but the total concentration of Fe within our samples was equivalent over all dust concentrations. We concluded that Fe dissolution is controlled by the Fe binding capacity of the seawater and, thus, ligand concentration and strength. To further investigate Fe dissolution from natural dust, we constructed two new experiments. In the first experiment we varied the ligand field within seawater with amendments of model ligands (oxalate, citrate, and aerobactin), while in the second we investigated the effects of sun light on aerobactin and seawater.

## 2. Method

### 2.1 Starting Materials

Two types of open ocean seawater were collected at 30°N, 140°W in November 2004 aboard the *R/V Melville* during the Sampling and Analysis of Iron (SAFe) intercomparison cruise. Surface seawater was collected with the University of California Santa Cruz (UCSC) trace metal clean surface “sipper” sampler (Bruland Lab), and sub-surface seawater was collected with the University of Hawaii’s 30 L GO-Flo niskin bottles at a depth of 24-26 m (Measures Lab). There was a 76 m mixed layer during sub-surface sampling; all relevant chemical and physical properties of the sub-surface water used in these experiments should be identical in the 24-26 m depth range. Sub-surface water was in-line filtered at sea through a 0.2 µm cartridge filter and stored in an acid leached 4 L polycarbonate (PC) bottle unacidified and in the dark. Surface water was in-line filtered at sea through a 0.4 mm cartridge filter and stored in a 25 L high-density polyethylene (HDPE) carboy, also unacidified in the dark.

Seawater from two separate coastal locations was collected and treated in two different ways. The first coastal seawater was collected at 10 m depth while at the Santa Monica Bay Observatory Oceanographic Mooring (33° 55.9’ N, 118° 42.9’ W) aboard the *R/V Seaworld UCLA* in December 2005. Sub-surface sample water was collected using Teflon

coated external spring niskin bottles with Teflon coated messengers (General Oceanics Inc. 1010X-5L) on ¼ inch polyester line. Water was pumped from the niskin bottle through a 0.2 µm cartridge filter (Sartobran cellulose acetate P 150) with a peristaltic pump using C-Flex tubing into a hepa-filtered work space. All sampling and laboratory materials were acid leached using trace metal clean techniques. The second coastal seawater was collected and UV irradiated at UCSC (Bruland Lab) as described in (Donat and Bruland, 1988), but using Biobeads SM-2 and Amberlite XAD-16 resins in lieu of their Sumichelate Q10R resin. Both coastal seawater samples were stored frozen in one or two liter Teflon PFA bottles.

The dust was a composite of 3 superficial deposits collected in natural dust traps in the Nevada desert (South-West of Las Vegas) (courtesy Marith Reheis, USGS). The dust was hand sieved through successive, clean polyethylene meshes of 100 and 20 µm pore diameter. The smallest fraction (<20 µm) was collected and stored in a clean glass bottle. It was then autoclaved to destroy any possible bacteria spores and stored in a dark cabinet. Elemental analyses of the dust show manganese (Mn), iron (Fe), and aluminum (Al) concentrations similar to crustal abundances (Wedepohl, 1995) (Table 1).

## *2.2 Experiment 1, Seawater Matrix*

The first experiment was designed to compare dust dissolution in different seawater matrices, focusing on the effects of model and natural Fe binding ligands. Open ocean surface seawater, Santa Monica Bay coastal seawater, UV irradiated coastal seawater, and UV irradiated seawater with added organic ligands were used in this experiment. Seven separate “seawaters” were prepared.

1. Santa Monica Bay coastal water, “Coastal Water”,
2. Open ocean surface seawater, “Open Ocean Water”,
3. UV irradiated coastal seawater (Bruland Lab UVSW), “UV Water”,

4. UV irradiated coastal seawater with the addition of citric acid (57 nM, Sigma-Aldrich Cat #25,127-5), “Citrate Water”,
5. UV irradiated coastal seawater with the addition of oxalic acid dihydrate (69.5 nM, Sigma-Aldrich Cat # 24,753-7), “Oxalate Water”,
6. UV irradiated coastal seawater with the addition of a combination of citric acid and oxalic acid dihydrate (57 nM & 69.5 nM, respectively), “Citrate & Oxalate Water”,
7. UV irradiated coastal seawater with the addition of aerobactin (EMC Microcollections) at a concentration of 50.1 nM, “Aerobactin Water”.

An initial sub-sample was taken from each bottle to measure dissolved metal concentrations (Mn, Fe) and Fe speciation including Fe-binding organic ligand concentrations and binding constants. Each sub-sample was taken by directly filtering, (0.2  $\mu\text{m}$  pore size, 25 mm polycarbonate Whatman) the sample seawater into a sub-sample bottle. Following each filtration, the filter was exchanged and the filter apparatus was rinsed with  $\sim 150$  mL water (18  $\text{M}\Omega$  cm) and 5 mL of the next sample. All metal concentration sub-samples were acidified with hydrochloric acid (12 M, SeaStar<sup>®</sup> HCl), and all Fe speciation sub-samples were sealed and frozen.

After sub-sampling ( $t=0$ ), the initial seven seawater samples were each split into two 1 L Teflon bottles, for a total of fourteen bottles. One bottle from each water type was sealed as a control, while the other bottle was saved for the dust addition. A mixture of 8.45 mg of dust and 52 mL of seawater was quickly shaken and then proportioned via pipette to each of the seven dust addition sample bottles in order to establish a dust concentration of 1.2 mg/L. This concentration is representative of typical dust deposition over ocean water (Duce and Tindale, 1991). Immediately following the addition of the dust, a sub-sample ( $t=30$  min to 2 hr 40 min) was taken from each bottle to measure the dissolved metal concentrations (Mn, Fe) and Fe speciation.

The sample bottles (including the control bottles) were sealed with parafilm, placed in clear zipper bags, and immersed in a 13°C water bath on the roof of the laboratory under a 50% light screen. The seawater samples were allowed to mature under the diurnal cycle for 28 days. Samples were removed from this bath on days 0.25, 0.5, 1, 2, 4, 7, 14, and 28 for ~2 hours to take sub-samples.

### *2.3 Experiment 2, Light Exposure*

The second experiment was designed to compare the dust dissolution effects of light on seawater, with and without amendments of the siderophore aerobactin, in order to elucidate the mechanism of siderophore-promoted dissolution. Two bottles of open ocean subsurface seawater (SAFe; see Starting Material) were used in this experiment. One bottle was left unaltered, “Seawater” while aerobactin was added to the second, “Aerobactin Water II.”

Aerobactin Water II was prepared by dissolving 1.088 mg of solid aerobactin in 1 mL of seawater. 111 µL of this solution was transferred to the seawater bottle via pipette to establish an aerobactin concentration of 51.1 nM. All work with solid aerobactin was conducted in an Ar filled glove bag in order to reduce any thermal oxidation and decomposition. Sub-samples of Seawater and Aerobactin Water II were then taken to measure initial metal concentrations (Mn, Fe) and dissolved Fe speciation.

A portion of both seawater types was poured into two different types of Teflon bottles. One bottle was translucent Teflon (the “Light” bottle), and the other was an identical bottle wrapped in black electrical tape to prevent light exposure (the “Dark” bottle). These four new samples became the “no dust” controls. A concentrated solution of dust in seawater (0.87 g dust/L) was added via pipette to the remaining Aerobactin Water II and Seawater samples to reach a dust concentration of 1.1 mg/L. Immediately following this addition, a

sub-sample was taken to measure initial Fe speciation. The samples were again partitioned into “Light” and “Dark” bottles, resulting in 8 total samples bottles: Seawater: light-no dust, dark-no dust, light-dust, dark-dust; and Aerobactin: light-no dust, dark-no dust, light-dust, dark-dust.

The Light bottles were sealed with parafilm and placed in a clear zipper bag, while the Dark bottles were sealed and placed in three brown bags to further reduce light exposure. All samples were immersed in a 13°C water bath on the roof of the laboratory under a 50% light screen. The samples were allowed to mature under the diurnal cycle for 18 days. Samples were removed from this bath on days 0.5, 1, 1.5, 2, 2.5, 3, 6, 9, and 18 for ~ 2 hours to take sub-samples.

#### 2.4 Analysis

All sub-samples were analyzed for dissolved Fe and Mn concentrations using a modified magnesium co-precipitation (MagIC) method (Wu and Boyle, 1998). This isotope dilution procedure concentrates the analyte by 20 fold, with isotope ratios measured on the Caltech Element I ICP-MS (Mendez *et al.*, in review). Dissolved Fe speciation, including both ligand concentration and binding strength, was measured using a competitive ligand exchange-adsorptive cathodic stripping voltammetry (CLE-ACSV) with the added ligand salicylaldoxime (Buck *et al.*, 2007).

#### 3. Results

The dissolution of Mn and Fe over time is shown in Figs. 2-5. In general, Mn concentrations increase to 3- 5 nM over the first three days (Figs. 2 & 4), and the pattern of increase was similar to previous experiments (Mendez *et al.*, in review). Mn concentrations in the Coastal Water were significantly higher than all other samples, starting at 4 nM and growing to nearly 7 nM (Fig. 2A). The Mn control samples showed no change over time in dissolved Mn concentration ([Mn] = 0.8 nM, Light experiment, < 0.1 nM all UV Waters, 0.7 nM Open Ocean Water, 4 nM Coastal Water).

Fe concentrations decreased to 0.2 – 0.8 nM over time after dust addition for Open Ocean Water, UV Water, Citrate Water, and Coastal Water (Fig. 3). The Oxalate Water sample had a large scatter in the data, and we could not determine any trends. Control samples showed over 50% loss of dissolved Fe, a majority of which occurred in the first week. The Light and Dark Seawater samples showed a moderate increase (2.0 - 2.5 nM) over the first two days, similar to our previous results (Fig. 5) (Mendez *et al.*, in review). All Aerobactin samples had a large increase in Fe concentration (~6 nM) peaking at 1 – 1.5 days after addition (Fig. 3 & 5). This concentration held constant for about 6 days before there was a noticeable decrease in dissolved Fe.

Error bars in Figs. 2-5 represent the precision of the calculated concentration and are  $2\sigma$  of the standard error. The isotope ratio of each sub-sample was measured on the ICP-MS. The standard error of this ratio was propagated along the concentration calculation to determine the precision. Accuracy was determined by measurements of archived samples from the Mediterranean, (Fe only, (Bonnet and Guieu, 2004)) and from the Pacific, (SAFe, (Johnson *et al.*, 2007)). While over 20 groups have analyzed the SAFe samples for Fe, only two groups have reported Mn concentrations. Table 2 reports a comparison between our measured concentrations and those of Bonnet (Table 2A), and those of the consensus concentration for the SAFe Fe concentrations and the two reported Mn concentrations (Table 2B).

A laboratory internal seawater standard was processed and analyzed along with these sub-samples to monitor consistency and accuracy over time. Over the course of these experiments, Fe concentrations were measured at  $0.060 \pm 0.049$  nM, n=55, which is well within the error of all other previous analyses of this standard, [Fe]  $0.085 \pm 0.063$  nM, n=145. Mn concentrations were measured at  $0.65 \pm 0.03$  nM, n=65 during this dissolution experiment; this is in agreement with all previous measurements that average  $0.66 \pm 0.06$  nM, n=165.

All samples from day 28 of the seawater matrix showed an increase in Fe concentrations compared to their previous sub-sample (day 14) (Fig. 3). Laboratory internal seawater standards and blanks measured along with these sub-samples showed no signs of contamination, indicating the sub-samples were most likely contaminated with Fe during sample collection.

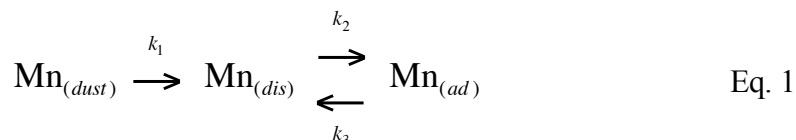
Ligand concentration and binding constants are reported in Table 3. Open ocean and coastal ocean water are within normal ranges for both concentration and Fe binding constants (Buck *et al.*, 2007; Rue and Bruland, 1995). Coastal Ocean and Aerobactin water were the only samples with multiple ligands types. Most samples had insignificant change or a reduction in ligand concentration over time; however, the dust addition sample for the UV irradiated water had a 56% increase in  $L_1$ . The binding constant for the aerobactin sample was  $\text{Log } K_1 = 11.5$ . A specific measurement of the  $\text{Log } K_{\text{FeL}}$  of aerobactin is 12.9 (Harris *et al.*, 1979), which is comparable our measurements. Because the Citrate & Oxalate Water sample was contaminated for Fe, its ligand binding capacity was not determined. A striking result is that the detectable oxalate ligand concentration was 30 nM before dust addition and 13 nM following dust addition. Open Ocean Water also had a decrease in detectable ligand concentration following dust addition; however, the other sample had such a large change in ligand concentration immediately following the dust addition.

#### 4. Discussion

##### 4.1 Manganese Kinetics

The pattern of Mn dissolution is similar to our previous experiments (Mendez *et al.*, in review) which showed fast initial dissolution followed by a leveling off to an equilibrium value. This earlier work had a Mn dissolution rate of 0.9 nmol Mn/(day·mg dust). Our current results give the same value, ( $0.88 \pm 0.13$  nmol Mn/(day·mg dust)) when averaged over a two day time period to match the previous coarse resolution. Further, in the current experiments the time resolution is fine enough to model the results and compute the initial dissolution rate as the first derivative at time zero.

We modeled our data with a two step reaction (Eq. 1): comprised of an irreversible dissolution of Mn from the dust and a reversible exchange reaction. The reversible reaction represents the combination of all the reversible reactions that exchange dissolved Mn with dust particles surfaces, dust particles, the bottle wall, other seawater colloids, and/or solid Mn oxides.



A differential equation was constructed and analytically solved for each Mn species. These solutions were used to find the best fit for the three independent variables,  $\text{Mn}_{dust}$ ,  $k_1$ , and  $k_2$ , to the sample data (the model details and the process used to model the data are described in Appendix 1). Using  $\text{Mn}_{dust}$ ,  $k_1$ , and  $k_2$ , we computed the first time derivative of  $\text{Mn}_{dis}$  and calculated the initial dissolution rate of Mn from the dust, by dividing by the dust concentration. The calculated dissolution rates are presented in figure 6.

Oxalate-promoted dissolution was significantly faster than the other seawater matrices (11.23 nmol Mn/day/mg dust, Fig. 6A). This enhancement has been previously described at lower pH and higher concentrations of both oxalate and solid Mn oxides than we use here (Jun and Martin, 2003; Stone and Morgan, 1984; Wang and Stone, 2006; Xyla *et al.*, 1992). We also measured a dramatic reduction in dissolved oxalate concentration after dust addition (Table 3), which we presume is due to the fast binding of oxalate to the mineral surfaces of the dust. This observation is similar to earlier work (Stone, 1987) describing the oxalate-promoted dissolution mechanism where the bidentate oxalate ion binds onto a Mn atom on the mineral surface, displacing two of the hydroxyl groups. This complexation weakens the metal-oxygen bonds which can then be broken upon further protonation, followed finally by dislocation of Mn from the mineral surface, or reduction and dislocation (Stumm and Morgan, 1996). Oxalate binding is known to inhibit proton-promoted dissolution by

blocking dissolution sites, reducing the rate by as much as an order of magnitude; however, this is only for the more soluble Mn(II) in acidic conditions (pH 2 – 5.6) (Banerjee and Nesbitt, 1999). At ocean pH, the proton-promoted dissolution is significantly slower (Stumm and Morgan, 1996). Oxalate-dissolution, on the other hand, is not prohibited at higher pH and is dependent on the concentration of surface adsorbed oxalate (Stone and Morgan, 1984). In addition, oxalate can promote the reductive dissolution of Mn (III) and Mn (IV) (Banerjee and Nesbitt, 1999; Xyla *et al.*, 1992), which may overcome any proton-promoted dissolution inhibited by oxalate. Our data from seawater support the conclusion that oxalate promotes Fe dissolution that has been previously shown in laboratory conditions.

A second clear conclusion is that light promotes Mn dissolution in our experiment (Fig. 6B). We see an increase in Mn dissolution rate in the illuminated samples of both the Seawater and Aerobactin Water. There was no significant difference between the Aerobactin Water and Seawater sample, which is consistent with our previous conclusion that Mn dissolution is only dependent on dust concentration. We previously proposed that Mn dissolution is due to both the release of soluble reduced Mn (II) mineral and the reduction of Mn (III) and Mn (IV) species in the mineral structure of the dust particles (Mendez *et al.*, in review). These new data further support this hypothesis, suggesting that Mn is not only dissolved from the dust particles by dissolution of Mn (II) and the reduction of oxidized Mn, but also photo-reduction of Mn (III) and Mn (IV) that increases the overall dissolution rate above the background solubility of the Mn phases (Fig. 6B).

The Coastal Water sample has a Mn dissolution rate about half that of the majority of the other samples (Fig. 6A), likely due to its large initial Mn concentration (Fig. 2B). Mathematically, our model calculates the increase in dissolved Mn and takes the derivative at time zero as part of the initial dissolution rate. In a system with no initial Mn, the irreversible dissolution proceeds alone and dissolved Mn grows in concentration. As the concentration builds, the exchange reaction develops, reducing the rate of increase until the

system reaches steady state. This model approach works well with low initial Mn concentrations. If the initial Mn concentration is large, the exchange reaction will occur at time zero, competing with the irreversible dissolution. In this case our dissolution rate is more representative of the total rate of change in dissolved Mn and not of Mn dissolution from the dust. Chemically, this means that when dust is added to a system in equilibrium, there is a fast irreversible dissolution releasing Mn and comparably fast exchange reactions re-establishing equilibrium with the new surface area of the dust.

The Mn dissolution rates of the other seawater samples were equivalent, with an average rate of  $3.82 \pm 0.83$  nmol Mn/day/mg dust (excludes the Oxalate Water, Coastal Water, and the two dark samples). While there were slight variations in these rates, they can be attributed to slight differences in initial Mn concentrations, scatter in the data, and slight chemical differences that cannot be distinguished here.

#### *4.2 Manganese Thermodynamics*

The dissolution reactions in both the seawater matrix and light experiment appeared to reach equilibrium after one week. The aerobactin samples in the light experiment, on the other hand, had a significant reduction in Mn concentration after day 6 (Fig. 4). Table 4 presents the initial and final Mn concentrations, the change in Mn as a percentage of the total dust Mn for both the data and the model, and the equilibrium constants calculated by the model (defined as  $K_{eq} = \frac{Mn_{ads}}{Mn_{dis}}$ ).

Initial examination of the data from the first experiment reveals that: 1) the  $K_{eq}$  values are very similar to each other and 2) with the exception of the Coastal Water, the percentages of Mn dissolution are nearly equivalent. The equilibrium constants are a measure of manganese stability in the dissolved phase compared to the adsorbed phase. Since all the sample  $K_{eq}$  values are clustered together (mean =  $0.59 \pm 0.14$ ) despite their different ligands and below one, we conclude that total Mn dissolution is largely a function of Mn seawater

solubility and not organic complexation, and that Mn prefers the dissolved phase over the adsorbed phase. Furthermore, because the percentages of the total dust Mn dissolution are similar (excluding the Coastal Water sample), we believe that total dissolution is driven more by available or accessible Mn than the presence of organic ligands. As an example, oxalate drove dissolution at a faster rate than the other samples, but its total dissolution was not enhanced. While equilibrium constants are important in systems where steady state is reached, it might not be as important in the surface ocean where transport processes and a rich assortment of organics could alter the equilibrium. Therefore, the redox processes and kinetic enhancement involving ligands are important to Mn cycling.

Two samples had  $K_{eq}$  values that were significantly different: the Open Ocean sample and the Citrate Water sample. The Open Ocean sample retained more dissolved Mn than any other sample, thus decreasing the equilibrium constant. This may have resulted from the assemblage of natural organic material present in the water. These natural organics can provide a continual oxidant supply which drives photo-reduction reactions maintaining the soluble Mn(II) concentration (Sunda *et al.*, 1983). The Mn concentration in the Citrate Water sample was consistently below all other samples (Fig. 2A). Citrate may act to hinder Mn release rather than as a reductive promoter of dissolution. Although citrate is known to promote Mn(III) dissolution at high concentration (50 mM, (Klewicki and Morgan, 1999)), our relatively small concentration of citrate (57 nM) may not be enough to promote Mn(III) dissolution to an appreciable amount and may act to reduce total dissolution by occupying surface sites. In addition, within an oxygenated system Mn(II)-citrate complexes can be oxidized to Mn(III) ten times faster than a Mn(II) bicarbonate solution at pH 8 (Klewicki and Morgan, 1998; von Langen *et al.*, 1997). Therefore, total dissolved Mn concentrations may be suppressed due to reoxidation within the Citrate Water sample.

The percentage of the dust Mn that dissolved into the Coastal Water is smaller than that of the other samples. While this may first appear as though less total Mn dissolved from

the dust, we attribute this lower percentage to the relatively high initial Mn concentration adsorbing onto the dust particles and the wall. Table 4 shows the calculated equilibrium constants ( $K_{eq}$ ) for our two step model. The Coastal Water equilibrium constant is within error of the mean of the other seawater matrix samples. Therefore, Mn has the same preference for the dissolved state within the Coastal Water as the other samples, and it will have the same total Mn dissolution from the dust. As Mn was released from the dust, a portion was adsorbed onto a surface. Because there was a large initial Mn concentration, a large quantity of Mn must adsorb onto a solid surface, resulting in a smaller percentage staying in solution.

Seawater in the light experiment behaved similarly to our seawater matrix experiment, although the Mn concentrations were smaller overall, which resulted in smaller percentages of the total dust Mn and larger  $K_{eq}$  values. The similarity in  $K_{eq}$  between the Seawater Light and Dark samples indicates that while photoreduction plays a role in the initial release of Mn, there is no process within these samples to keep Mn in solution after the first two days. Aerobactin Water Dark and Light samples were not similar to each other; instead, the Mn concentration in the Dark sample decreased to nearly half that of the Light sample. It is plausible that the lack of light resulted in slow oxidation of Mn into one of its insoluble oxidized forms; however, the Seawater does not behave in this manner. This difference leads us to the conclusion that aerobactin is preventing Mn from interacting with reductive organics present in the seawater, perhaps by temporally stabilizing Mn(III), leading to its greater adsorption to the wall or particles over time. Mn(III) is a high spin trivalent ion with ionic radii equivalent to Fe(III) (Stone, 1987) and may be able to weakly substitute into the siderophore complex similar to chromium (Raymond and Carrano, 1979). Without light to continually reduce the oxidized species back to Mn(II), perhaps this weak interaction leads to overall loss of Mn from solution.

The seawater matrix and the light experiment differ in their final Mn concentrations, resulting in different  $K_{eq}$  values. Both experiments used U.S. dust of approximately 1 mg

dust / L, but the seawater matrix experiment yielded a larger final Mn concentration. Our previous experiment (Mendez *et al.*, in review), in which we compared dust concentrations, was more similar to the light experiment and showed smaller final Mn concentrations for the equivalent dust concentration. The most significant difference between these experiments is the time of year during which they were performed. Both the light experiment and the dust concentration experiment were conducted in August, while the seawater matrix experiment was conducted in January and February. It is possible that the greater UV exposure during the winter months lead to the larger Mn concentrations, resulting from an increased rate of photoreduction of re-oxidized Mn. While this seems like a plausible explanation for the difference between the dust concentration and the seawater matrix experiments, it does not explain the similarity between the Seawater Light and Dark samples in the light experiment. If the decrease in UV light during the summer reduced the final Mn concentrations in the dust concentration experiment, then removing UV light from the system should have further decreased this effect, which was not observed.

#### *4.3 Iron Dissolution*

The seawater matrix experiment demonstrates the dramatic effect of siderophores on the dissolution and retention of dissolved Fe (Fig. 3 & 5). Aerobactin Water had a large increase in Fe concentration, while the Open Ocean, Coastal, and Citrate Water had small increases in Fe. Fe concentrations declined in UV Water. Although oxalate promoted Mn dissolution, changes in dissolved Fe were not observed given the scatter in this experiment's data.

The ultimate reduction of Fe concentration below initial values in all samples except the aerobactin was initially contradictory to our previous experiment. However, as we will show, the differences in experimental set-up and materials can account for the dramatic differences. The small increases in Fe concentration within the first 12 hours of the experiment are also important to understand. Although the increases are not significant in the long term results of our bottles studies, we will explain that within the surface ocean,

this initial Fe release may play an important role for the biological community. The Aerobactin Water sample has a dramatic increase in Fe concentration, which takes several days to develop. We will lastly discuss the importance of this result to dust deposition as a source of Fe to the surface ocean, and then continue with the discussion of siderophore-promoted dissolution mechanism.

Open Ocean Water (same source as (Mendez *et al.*, in review)) showed Fe release to a maximum concentration of 1.0 -1.25 nM within the first 12 hours, followed by a decrease to 0.25 nM. Mendez *et al.* (in review), on the other hand, found Fe concentrations between 1.5 – 2.0 nM. This difference is most likely due to the change in the natural ligand complexing capacity during 11 months of storage in our lab. Ligand strength measurements made at the time of water collection were:

$$[L_1] = 1.67 \pm 0.03 \text{ nM (log } K_1 = 12)$$

$$[L_2] = 3.2 \pm 0.1 \text{ nM (log } K_2 = 11) \quad (\text{Buck, K.N., unpublished data})$$

The ligand assemblage in the Open Ocean Water sample at the beginning of the experiment had a larger  $L_1$  concentration than the at sea measurements, but the binding constant was lower and there was no  $L_2$  ligand (Table 3). To quantitatively understand why the results in this experiment were so different, compared to Mendez *et al.*, (in review), we define the iron binding capacity as the maximum quantity of Fe which can be held in solution. To calculate the total Fe binding capacity of this sample, we assume that ligands bind Fe according to the following reaction:



where the Fe binding capacity is  $[FeL]$ ,  $[Fe]$  is the inorganic Fe concentration in seawater (0.1 nM) and L is the unbound ligand. The Fe speciation measurement represents both the

bound and unbound ligand ( $FeL + L$ ); therefore, to calculate just  $[FeL]$  we write the equations:

$$K = \frac{[FeL]}{[Fe][L]} \quad \text{Eq. 3}$$

$$L_T = [FeL] + [L] \quad \text{Eq. 4}$$

where  $K$  is the Log of the binding constant (Table 3) and  $L_T$  is the Fe speciation measurement. Combining equations 3 and 4, we get the equation for Fe binding capacity:

$$[FeL] = \frac{L_T}{\left(1 + \frac{1}{10^K Fe}\right)} \quad \text{Eq. 5}$$

The  $FeL$  binding capacities for the natural seawater matrices are shown in Table 5. Looking at these natural waters we see that the pre-dust open ocean seawater from Mendez *et al.*, (in review) is dramatically under-saturated with respect to the concentration of ligands, yielding a  $FeL_T / [Fe]$  ratio of over 18 (Table 5). Therefore, once dust was added, the dust-bound Fe was quickly released, raising the concentration to 1.5 nM. In contrast, the aged and slightly contaminated open ocean seawater had about half the Fe binding capacity and an Fe concentration of over 1 nM. This seawater was not under-saturated in Fe and so there was no dramatic increase in Fe concentration upon dust addition as there was in Mendez *et al.* (in review). In fact, the decrease in Fe is most likely due to the adsorption of initial Fe and ligands onto the container wall or dust particles themselves. The Coastal Water sample yields a very similar result. Coastal Water is not under-saturated in Fe with respect to the Fe binding ligands, and therefore, over time, some of the initial Fe is adsorbed onto the wall of the bottle, reducing the Fe concentration.

The Fe concentration in both the Open Ocean and Coastal Water, as well as the Citrate Water, increased during the first 24 hours; however, the rate of Fe dissolution was

impossible to measure. In each case, this initial increase in Fe concentration was followed by the large decreases described above. These initial increases may be attributed to the dissolution of Fe solubilized by ligands found in the waters (Voelker *et al.*, 1997) or the release of soluble Fe(II) bound to the dust (Pehkonen *et al.*, 1993). Despite the fact that the dust addition did not ultimately increase the Fe concentration, our data show that there is soluble Fe on these dust particles. Leaching experiments by (Buck *et al.*, 2006) showed that there was significant quantities of soluble Fe which could be released from aerosol particles given the right conditions. In these experiments Buck *et al.*, (2006) used ultra-pure water (18 M $\Omega$  cm) to remove Fe from the aerosol particles. Although Fe is more soluble in pure water, compared to seawater, they reason that surface microlayer conditions may solubilize Fe to a greater degree. Therefore, pure water is a good substitute for the surface microlayer. However, our data show that unaltered seawater can leach more Fe from the dust particles than is soluble over time. This initial Fe may quickly overwhelm the surrounding ligand field and thus begin the precipitate. However, in the complete system of the surface ocean, the reservoir of available ligands would be less likely to become saturated and that initial Fe would not precipitate. Within the surface ocean this initial Fe release is part of the dust source linked to the Fe cycle and should not be ignored.

The Fe concentration within the Aerobactin Water increased to  $5.92 \pm 0.13$  nM 50 hours after dust addition (Fig. 3). Using the initial linear portion of the curve, we calculate a rate of dissolution of  $2.25 \pm 0.18$  nM Fe/day/mg dust. This is the first experimental evidence of a siderophore facilitating Fe dissolution from a natural dust in natural seawater. Siderophores produced by marine bacteria (*Alteromonas haloplanktis*) have been shown to promote hematite as well as amorphous Fe hydroxide dissolution under acidic conditions and micromolar siderophore concentrations (Yoshida, 2002). In addition, dissolution rates for goethite and poorly crystalline Fe hydroxides at pH 8 were below detection limit ( $<0.5$   $\mu$ M Fe). Siderophores (DFOB and aerobactin) have been shown to dissolve goethite and lepidocrocite at pH 4 in millimolar siderophore concentrations (Hersman *et al.*, 1995), and

pH 5-6 with 45 - 80  $\mu\text{M}$  siderophore concentration (Borer *et al.*, 2005; Cheah *et al.*, 2003). In each of these studies Fe oxide dissolution is proportional to siderophore concentration, although an extrapolation towards nanomolar concentrations of siderophore was not dissimilar from controls. Our experiments prove that not only can siderophores promote Fe oxide dissolution under optimal laboratory conditions, but that they promote Fe dissolution from natural mineral aerosols in ocean water. This means that siderophore promoted dissolution may be one mechanism for Fe to be released from dust upon dry deposition to the surface ocean. Although scenarios involving micro-environment changes can be useful in facilitating additional Fe dissolution, given the concentrations of Fe binding ligands found in the surface ocean (Buck *et al.*, 2007) they may not be necessary.

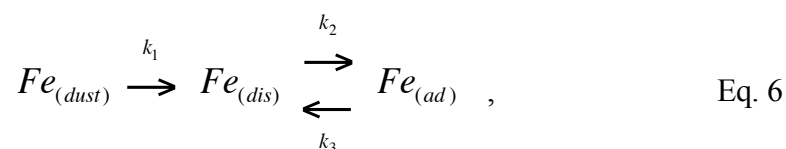
#### *4.4 Effects of Light Exposure on Iron Release*

There is already substantial knowledge of the mechanism for Fe oxide dissolution in the literature, however the interactions between dust, siderophores, and a natural seawater matrix has not been investigated. Here we discuss the data from our experiment and compare it to several other studies to further understand siderophore-promoted dissolution. We designed the light exposure experiment to elucidate certain mechanistic components of siderophore-promoted dissolution of Fe oxides.

If aerobactin can dissolve Fe oxide minerals through a photolytic mechanism as described in the literature, a dissolution experiment comparing light and dark samples should have two results. The Aerobactin Light sample should proceed faster than a Dark sample and the relative increase in dissolution between light and dark samples should be greater for the Aerobactin sample than for the Seawater sample. Unaltered seawater may have light-promoted Fe dissolution from thermal or photo-reductive pathways of surface Fe(III)-hydroxy groups, excitation of the  $\text{O}^{2-} \rightarrow \text{Fe}^{3+}$  charge transfer band with reduction of the surface Fe(III) (Borer *et al.*, 2005), or photolytic reduction involving natural ligands (Waite and Morel, 1984). If the relative dissolution rate increase due to light exposure is equivalent

between the Aerobactin and Seawater samples, the dissolution increase may be attributed to these processes rather than siderophore photolytic dissolution.

Our light experiment showed that total Fe dissolution was affected by light exposure, and aerobactin reactivity did appear to be enhanced by light more than unaltered seawater. The light experiment results were analyzed using a similar reaction for Fe as was applied to Mn,



to model the kinetics of Fe release and retention in solution. Just as with the Mn system, we constructed three differential equations for each of the species, and solved them analytically. The time derivative of the  $Fe_{dis}$  equation at time zero was then used to compute the dissolution rate. For the Fe system here we first used the controls to constrain the ratio of the adsorption and desorption reaction constants and thus solve for one of the independent variables. Using these constraints we then solved the dissolution reactions by fitting the other two independent variables to the data (Appendix 1 has a complete description of the model). Figure 7 shows the rate of initial dissolution for each of the four dissolution reactions.

Fe dissolution in both light exposed samples was faster than their corresponding darks samples. However, the increase in Fe dissolution for the Aerobactin Light sample was  $2.1 \pm 0.3$  times that of the dark sample, where as the Seawater Light sample only increased by  $1.1 \pm 0.4$  times. Because the relative rate increase was larger in the Aerobactin Light sample, we must consider that beyond thermal dissolution there was one or more photolytic dissolution processes at work in the Aerobactin sample or both the Seawater and Aerobactin samples. We can compare our results to those of Borer *et al.*, (2005) to determine the likelihood of light promoted aerobactin dissolution, and to Cheah *et al.*, (2003) to understand the relative rate increase in the aerobactin samples.

(Borer et al., 2005) examined the aerobactin-promoted Fe oxide dissolution mechanism and concluded that aerobactin is not light sensitive. They determined that aerobactin dissolution begins with adsorption of one of the hydroxamate binding groups and follows the mineral dissolution mechanism outlined by Zinder *et al.*, (1986). Borer *et al.*, (2005) reason that because the rate of ligand controlled Fe oxide dissolution is linearly proportional to the ligand binding constant (Duckworth and Martin, 2001) and only one binding group will adsorb onto the mineral surface at a time (Borer et al., 2005; Coccozza et al., 2002), the rates of dissolution may be used as a proxy for ligand-surface binding constants. Examination of the aerobactin Fe oxide dissolution rate can lead to the aerobactin-surface binding constant, which will depend on which one of the binding groups adsorbs to the Fe oxide surface, one of the hydroxamate groups or the  $\alpha$ -hydroxycarboxylate. The other binding groups are sterically restricted from involvement and will bond once the Fe is removed from the lattice structure. Fe-hydroxamate binding constants are stronger than similar Fe- $\alpha$ -hydroxycarboxylate, [the Fe stability constant for acetohydroxamic acid (a simple hydroxamic acid) is 8 orders of magnitude larger than for glycolic acid (a simple  $\alpha$ -hydroxycarboxylic acid) (Smith *et al.*, 2004)]. In Borer *et al.*, (2005), both aerobactin and DFOB (a tri-hydroxamate siderophore) have a similar dark lepidocrocite dissolution rate, and both have a 4.1 fold increase in dissolution rate upon light exposure. Because DFOB has no light reactivity (Barbeau, 2006), they conclude that the increase in Fe dissolution is caused by the photo-reactivity of the Fe oxide surface and not by a photo-induced reaction of the adsorbed siderophore. This indicates that aerobactin and DFOB have the same binding group, hydroxamate, and that aerobactin does not photoreactively dissolve Fe oxides. There is a 40% difference between the lepidocrocite dissolution rate of DFOB and aerobactin, but because both the light and dark dissolution rates have the 40% difference, it is believed that this is the result of a non-photoreactive property of the siderophores.

The light and dark dissolution rates calculated by Borer *et al.*, (2005) as well as the dissolution rates calculated for both our Light and Dark - Aerobactin and Seawater samples

are presented in Table 6. The two studies used different units to report their dissolution rates; therefore, to properly compare, we converted the units of Borer *et al.*, (2005) using the conversion,  $170 \text{ m}^2/\text{g}$  (P. Borer, per. comm.). In addition, dissolution experiments in Borer *et al.*, (2005) were conducted in pure water and had no background ligand field. Their control had no Fe dissolution. Therefore, all dissolution in their aerobactin experiment is due to the siderophore. Our background seawater had significant Fe dissolution. Therefore, the dissolution rate in our aerobactin sample was a composite of both aerobactin and the natural seawater ligands. To properly compare our results we need to take the absolute difference of our Aerobactin and Seawater samples to remove the effects of the seawater's background ligand field. Finally, since ligand-controlled dissolution is a function of the surface excess of adsorbed ligand (Furrer and Stumm, 1986), we divided our absolute difference rates and the converted rates of Borer *et al.*, (2005) by the total aerobactin concentration.

The calculated dissolution rates from both this study and Borer *et al.*, (2005) are similar despite significant differences in experimental set-up. Borer *et al.*, (2005) used synthesized colloidal Fe oxide (lepidocrocite) in an acidic buffered solution with micromolar concentrations of both siderophore and Fe. We used a natural dust in ocean water at pH 8 with nanomolar Fe and siderophore concentrations. This is an important finding because the similarity in our dissolution rates indicates that initial aerobactin-promoted Fe oxide dissolution is controlled by ligand adsorption to the mineral surface and is not appreciably influenced by proton-promoted dissolution or the dissolution effects of other natural organic ligands.

If aerobactin-promoted Fe oxide dissolution is not specifically photoreactive, and the light enhancement in dissolution was from mineral surface reactions, as was concluded by Borer *et al.*, (2005), then the same mineral surface reactions which occurred in the Aerobactin Light sample should occur in the Seawater Light sample. But as described above, the relative rate increase in the Aerobactin Light sample was larger than the relative rate increase

seen in the Seawater Light sample. Thus, if these surface reactions occurred in the Seawater Light sample they had a diminished effect on Fe dissolution. One explanation of the observation to not use a photoreactive mechanism was outlined by Cheah *et al.*, (2003).

(Cheah *et al.*, 2003) observed that slight additions of a siderophore (*e.g.* DFOB) in combination with another organic ligand (*e.g.* oxalate) will lower the  $\Delta G$  of the Fe oxide dissolution. They proposed that the undersaturation with respect to the mineral caused by the siderophore's large binding constant and high specificity for Fe will allow other organic ligands to act as a dissolution catalyst. After the ligand removed an Fe atom from the mineral surface, the siderophore would take the Fe away from the smaller ligand and act as a reservoir. Thus, it has been proposed that one function of siderophore production in Fe limited environments is to facilitate other dissolution mechanisms by lowering the solution saturation state (binding free Fe ions and altering the overall thermodynamic equilibrium) (Cocozza *et al.*, 2002; Holmen and Casey, 1996; Kraemer, 2004). However, this was an observation in an acidic environment where, due to protonation, oxalate is more effective at binding to and detaching Fe from Fe oxide surfaces (Cheah *et al.*, 2003). In the oceanic environment (pH ~8), protonation of the oxalate ligand and subsequent detachment of the Fe-oxalate complex from the Fe oxide surface is less likely (Zinder *et al.*, 1986) and, thus, not a likely scenario for oxalate. However, other more effective ligand may be present in natural seawater. The observation by Cheah *et al.*, (2003) may explain the relative rate increase seen in our Aerobactin Light sample. In our experiment, the natural assemblage of organics had a 12% increase of Fe dissolution upon exposure to the light. When aerobactin was added to the water, we saw a 107% increase in Fe dissolution. This effect may be due to the siderophore binding Fe, which otherwise would have been re-oxidized in the natural water system. This suggests that by trapping dissolved Fe as it is removed from the mineral, preventing any re-oxidation and precipitation from solution aerobactin, promotes photodissolution without being photoreactive itself as concluded by Borer *et al.*, (2005).

#### 4.5 Iron Thermodynamics

The long-term decrease in Fe concentration in the aerobactin sample was most likely due to multiple adsorption reactions. From the Aerobactin Water in the seawater matrix experiment we saw a 50% reduction in total dissolved Fe after 28 days. Most of the reduction occurred within the second week of the experiment. We hypothesized that this reduction was due to the destruction of the aerobactin ligand through decomposition or adsorption to a surface (the wall or dust particle). Examination of the aerobactin samples in the light experiment showed similar dissolved Fe loss over time with significant loss between days 6 and 9. There was only a slight difference between the lit and dark aerobactin samples, leading us to conclude that any photodecomposition of the siderophore is minor. (Küpper *et al.*, 2006) found that the aerobactin-Fe complex is photoreactive but stable. They determined that the photo-product has a Fe binding constant which is slightly stronger than the parent aerobactin ligand ( $\text{Log } K = 27.6 \pm 0.1, 28.6 \pm 0.5$  for aerobactin and the aerobactin photo-product respectively).

Direct loss of the Fe-aerobactin complex may occur through adsorption to the bottle wall, or the surface of the dust particles. Adsorption to bottle wall is reduced by “conditioning” sample bottles with sample. Adsorption of the aerobactin-Fe complex to dust or other large particles (filterable at 0.2 mm) is the other explanation for Fe loss over time. The non-Fe binding carboxyl groups can allow aerobactin to re-adsorb to mineral surfaces after Fe complexation (P. Borer, pers. comm.). During Fe dissolution experiments this results in a nonlinearity due to outer sphere adsorption of aerobactin-Fe complexes to the Fe oxide mineral.

## 5. Conclusions

Dry deposition of dust is a substantial source of both Fe and Mn to the surface ocean (Duce and Tindale, 1991; Guieu *et al.*, 1994). However, the pattern of Fe and Mn dissolution is significantly different. In our experiments, Mn dissolution occurred over the course of several days until the available Mn is depleted and reached a steady state concentration. The rate of Mn dissolution was enhanced by the bidentate ligand oxalate,

but the total quantity of Mn dissolution was not affected. Light also enhanced the Mn dissolution rate, and comparing the final Mn concentrations of both experiments we see that the level of atmospheric radiation lead to differences in the final steady state Mn concentration.

Fe dissolution is highly dependent on the background seawater ligands. Depletion of these ligands lead to the precipitation of Fe oxide from solution, while additions of siderophores enhanced both the total Fe capacity of the seawater and the rate of Fe dissolution from dust. The mechanism of aerobactin-promoted dissolution can be described in terms of bidentate ligand dissolution without a specific photolytic step. Photo-induced dissolution was promoted in both our Seawater and Aerobactin samples. While the relative rate increase was more significant in the Aerobactin sample, this can be explained by siderophore complexation of Fe(III) removed from the mineral surfaces by weaker seawater ligands. Therefore, the reduction of Fe(III) at the mineral surface occurring in amended seawater was transferred to the bulk solution, while Fe(III) in the non-amended seawater reoxidize and remained on the mineral surface. While the Fe-aerobactin complex is photoreactive, there does not appear to be an aerobactin photoreactive dissolution mechanism.

## TABLES

	U.S. Dust	Upper Crust, Wedepohl, 1995
Manganese, (Mn)	750 ppm	527 ppm
Iron, (Fe)	3.81 %	3.1 %
Aluminum, (Al)	7.58 %	7.7 %

Table 1: Elemental analysis of the dust samples used in the dissolution experiment. Measurements are total metal mass concentrations.

(A)		[Fe], nM			
Mediterranean		Our Measurement		Bonnet	
Sample 1		1.41		1.37	
Sample 2		0.87		0.83	
Sample 3		1.31		0.89	

(B) Pacific	[Fe], nM		[Mn], nM		
	Our Measurement	Consensus	Our Measurement	Middag and de Baar, NIOZ	Wu, University of Alaska, Anchorage
SAFe, S1	$0.084 \pm 0.017$	$0.097 \pm 0.043$	$0.72 \pm 0.06$	$0.73 \pm 0.01$	$0.90 \pm 0.02$
SAFe, D2	$0.93 \pm 0.10$	$0.91 \pm 0.17$	$0.32 \pm 0.03$	$0.295 \pm 0.007$	$0.45 \pm 0.11$

Table 2: Comparison in dissolved Fe measurements for three Mediterranean seawater samples provided by Cecile Guieu (Laboratoire d'Océanographie de Villefranche) (A), and dissolved Fe and Mn measurement for the two Pacific SAFe standards for (B). We report our average measurements of Fe and Mn for the SAFe samples along with the consensus values for Fe, and the two other reported measurements of Mn.

	[Fe], (nM)	[L <sub>1</sub> ], (nM)	K <sub>1</sub>	[L <sub>2</sub> ], (nM)	K <sub>2</sub>
<b>UV Water</b>					
Pre-dust	0.72	2.5±0.1	11.3	NA	NA
Control Day 28	0.18	2.4±0.3	11.59±0.05	NA	NA
Post-Dust 30 min	0.79	NA	NA	2.3±0.5	10.89±0.04
Post - Dust 28 days	1.41	NA	NA	3.6±0.4	10.35±0.1
<b>Oxalate Water</b>					
Pre-dust	0.65	NA	NA	30±1	10.11±0.04
Control Day 28	0.85	NA	NA	16.7±1.5	10.76±0.01
Post-Dust 30 min	0.82	NA	NA	12.93±0.1	10.5
Post - Dust 28 days	0.85	NA	NA	5.15±0.1	10.82±0.03
<b>Aerobactin Water</b>					
Pre-dust	3.13	26.0±1.5	11.53±0.1	13±1.0	10±0.2
Control Day 28	2.86	7.8±1	11.4±0.2	NA	NA
Post-Dust 30 min	3.1	30.8±0.1	11.8	18.4±0.8	10
Post - Dust 28 days	2.31	NA	NA	20.5±1	10.6±0.03
<b>Citrate Water</b>					
Pre-dust	0.68	4.05±0.1	11	NA	NA
Control Day 28	0.19	NA	NA	10.1±0.7	10.48±0.05
Post-Dust 30 min	0.84	NA	NA	NA	NA
Post - Dust 28 days	0.67	NA	NA	17±1	10.66±0.01
<b>Open Ocean Water</b>					
Pre-dust	1.04	7.1±1	11.54±0.01	NA	NA
Control Day 28	0.16	3.5±0.8	10.95±0.2	NA	NA
Post-Dust 30 min	0.82	1.9±0.2	11.75±0.05	NA	NA
Post - Dust 28 days	1.2	1.6±0.1	12.18±0.03	NA	NA
<b>Coastal Water</b>					
Pre-dust	2.24	5.4±0.2	11.65±0.06	2.5±0.4	10.85±0.02
Control Day 28	1.69	3.1±0.1	12.47±0.08	2.2±0.1	10.88±0.04
Post-Dust 30 min	2.68	6.5±0.1	11.9	NA	NA
Post - Dust 28 days	1.51	6.4±0.4	11.2±0.1	NA	NA

Table 3: Fe speciation data of the six water samples from the seawater matrix experiment. The Oxalate and Citrate water was not measured due to the large Fe contamination. The distinction between L<sub>1</sub> and L<sub>2</sub> is made by the strength of the binding constant.

Sample	Initial [Mn], nM	Final [Mn], nM	Data: $\Delta$ [Mn], % of total $Mn_{dust}$	Model: $\Delta$ [Mn], % of total $Mn_{dust}$	$K_{eq}$
<b>Seawater Matrix Experiment</b>					
Open Ocean	0.68	4.60	24.7%	24.2%	$0.37 \pm 0.06$
Coastal Water	4.18	5.64	9.2%	12.1%	$0.60 \pm 0.08$
UV Water	0.00	3.54	22.6%	22.7%	$0.54 \pm 0.06$
Oxalate Water	0.01	3.26	20.5%	22.3%	$0.56 \pm 0.11$
Citrate Water	0.02	3.03	18.9%	19.4%	$0.79 \pm 0.04$
Aerobactin Water	0.34	3.41	19.3%	20.2%	$0.68 \pm 0.09$
<b>Light Experiment</b>					
Aerobactin-Dark	0.75	1.64 (2.53)	6.0% (12.0%)	8.8%	$1.96 \pm 0.27$
Aerobactin-Light	0.75	2.57 (2.71)	12.3% (13.2%)	13.1%	$1.25 \pm 0.15$
Seawater-Dark	0.75	3.37	17.1%	15.8%	$0.95 \pm 0.03$
Seawater-Light	0.75	3.27	16.5%	15.3%	$0.99 \pm 0.12$

Table 4: Final Mn dissolution values for all seven samples. Initial and Final [Mn] are an average of the pre-dust [Mn] (n=3) and the [Mn] from day 28 (Seawater Matrix Experiment) or day 18 (Light Experiment) (n=2). The  $\Delta$ [Mn] values are the final changes in [Mn] as a percentage of the total dust Mn for both the actual data and the two-step model.  $K_{eq}$  is the equilibrium constant defined as the adsorbed Mn over the dissolved Mn. Data in parenthesis are from day 3; [Mn] fell after this point in the Aerobactin samples. Therefore, day 3 represents a maximum in the dissolved Mn concentration and thus should be used to calculate the amount of Mn released from the dust particles.

Sample	Fe <sub>L1</sub> , nM	Fe <sub>L2</sub> , nM	Fe <sub>Lr</sub> , nM	[Fe] <sub>i</sub> , nM	Fe <sub>Lr</sub> /[Fe]	
Mendez <i>et al.</i> 35 <sup>th</sup> day	Pre-Dust	1.65 ± 0.03	2.91 ± 0.09	4.56 ± 0.1	0.25 ± 0.13	18.25 ± 9.5
					1.51 ± 0.39	3.04 ± 0.78
Coastal Ocean 28 <sup>th</sup> day	Pre-Dust	5.28 ± 0.2	2.19 ± 0.34	7.47 ± 0.39	2.29 ± 0.07	3.26 ± 0.20
		6.02 ± 0.2	0	6.02 ± 0.84	1.38 ± 0.19	4.36 ± 0.66
Open Ocean 28 <sup>th</sup> day	Pre-Dust	6.9 ± 0.001	0	6.9 ± 0.001	1.03 ± 0.02	6.7 ± 0.95
		1.59 ± 0.07	0	1.59 ± 0.07	0.23 ± 0.02	6.91 ± 0.74

Table 5: Fe binding capacity for the natural seawater samples, as calculated by equation 5. The total Fe binding capacity, Fe<sub>Lr</sub>, is the sum of Fe<sub>L1</sub> and Fe<sub>L2</sub>, and represents the total potential dissolved Fe for the sample. The ratio Fe<sub>Lr</sub>/Fe is a measure of the under-saturation of Fe compared to the total Fe binding capacity. The water used in our previous study had an initial under-saturation of 18 times the initial [Fe]. This under-saturation lead to the Fe dissolution, resulting in much smaller under-saturation after 35 days, calculated by using the initial Fe<sub>Lr</sub> and the final [Fe]. The Open Ocean and Coastal Water samples began with a small under-saturation, and over the course of the experiment they both became more under-saturated.

This Study	$\frac{nmol Fe}{min \cdot m^2}$	$\frac{nmol Fe}{day \cdot g Dust}$	$\frac{mol Fe}{min \cdot g_{particle} \cdot mol aerobactin}$
Aerobactin – Dark		$3.31 \pm 0.12$	
Aerobactin – Light		$6.85 \pm 1.0$	
Seawater – Dark		$1.79 \pm 0.34$	
Seawater – Light		$2.00 \pm 0.57$	
Difference – Dark		$1.52 \pm 0.21$	$43 \pm 12$
Difference – Light		$4.84 \pm 0.66$	$137 \pm 37$
Borer <i>et al.</i> 2005			
Aerobactin – Dark	2.8	685	21.9
Aerobactin – Light	11.5	2815	90.1

Table 6: We present the initial Fe dissolution rates from our current study. Listed are the Aerobactin Water samples, the Seawater samples, as well as the “Difference” between Aerobactin and Seawater sample. Also listed are the aerobactin dissolution rates from Borer *et al.*, (2005), in both their original units ( $nmol Fe min^{-1} m^{-2}$ ) and the units used in this text ( $170 m^2/g$  - conversion factor from P. Borer per. comm.) to more effectively compare to our data. Because dissolution rate is a function of adsorbed ligand concentration, we list the dissolution rates divided by the aerobactin concentration used in each experiment: 51 nM in our study and 45  $\mu M$  for Borer *et al.*, (2005).

## FIGURES

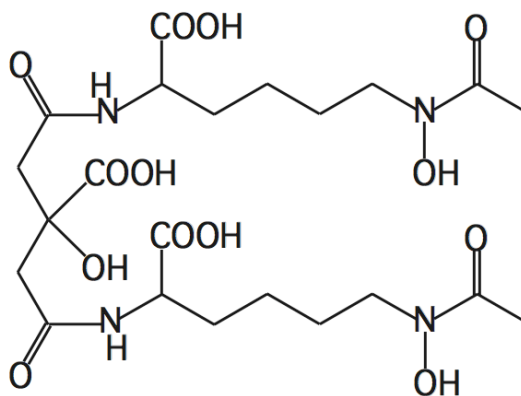


Figure 1: The Fe binding siderophore aerobactin. Aerobactin is a di-hydroxamate  $\alpha$ -hydroxy-carboxylate siderophore. Bonding to the Fe atom is done by the end hydroxamate groups and the center citrate moiety (Harris *et al.*, 1979).

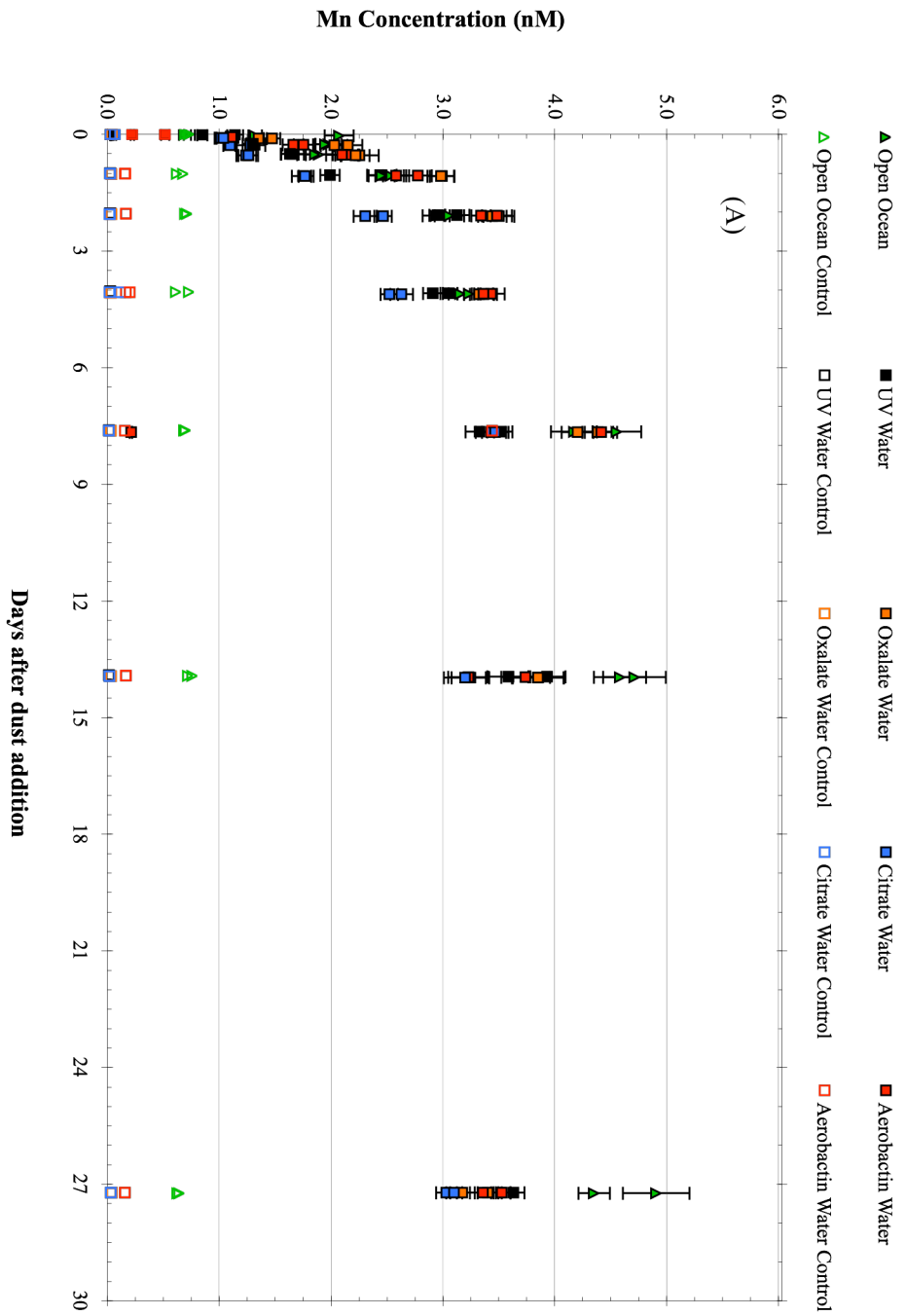


Figure 2: Mn concentrations over time for the seawater matrix samples: Open Ocean Water and all amended water samples A, and Coastal Water B. All samples are presented with their control samples. Error bars are two  $\sigma$  of the standard error of the mean computed from the isotope dilution equation. Error bars were removed from some control samples for clarity, and are smaller than the symbols.

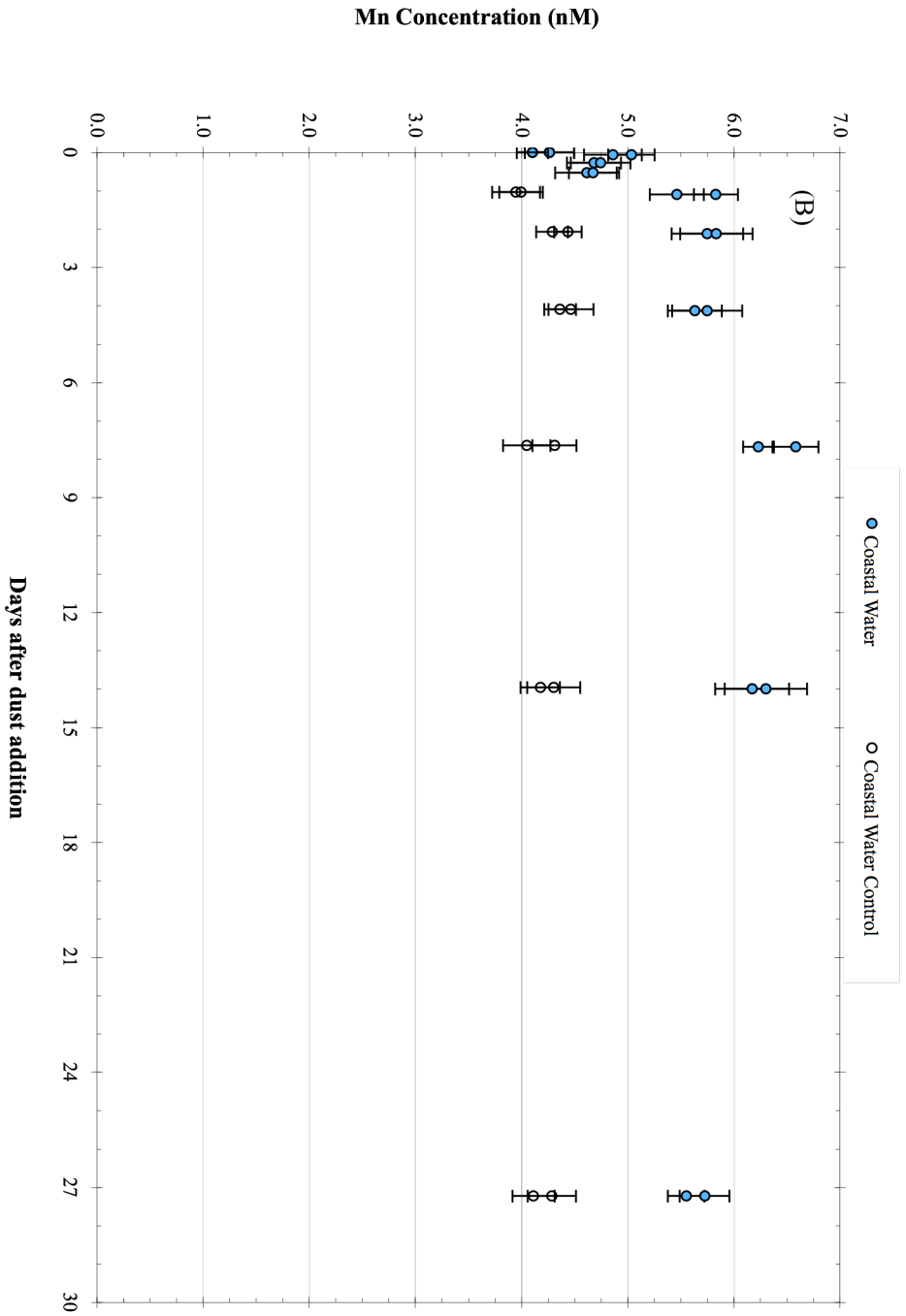


Figure 2: Mn concentrations over time for the seawater matrix samples: Open Ocean Water and all amended water samples A, and Coastal Water B. All samples are presented with their control samples. Error bars are two  $\sigma$  of the standard error of the mean computed from the isotope dilution equation. Error bars were removed from some control samples for clarity, and are smaller than the symbols.

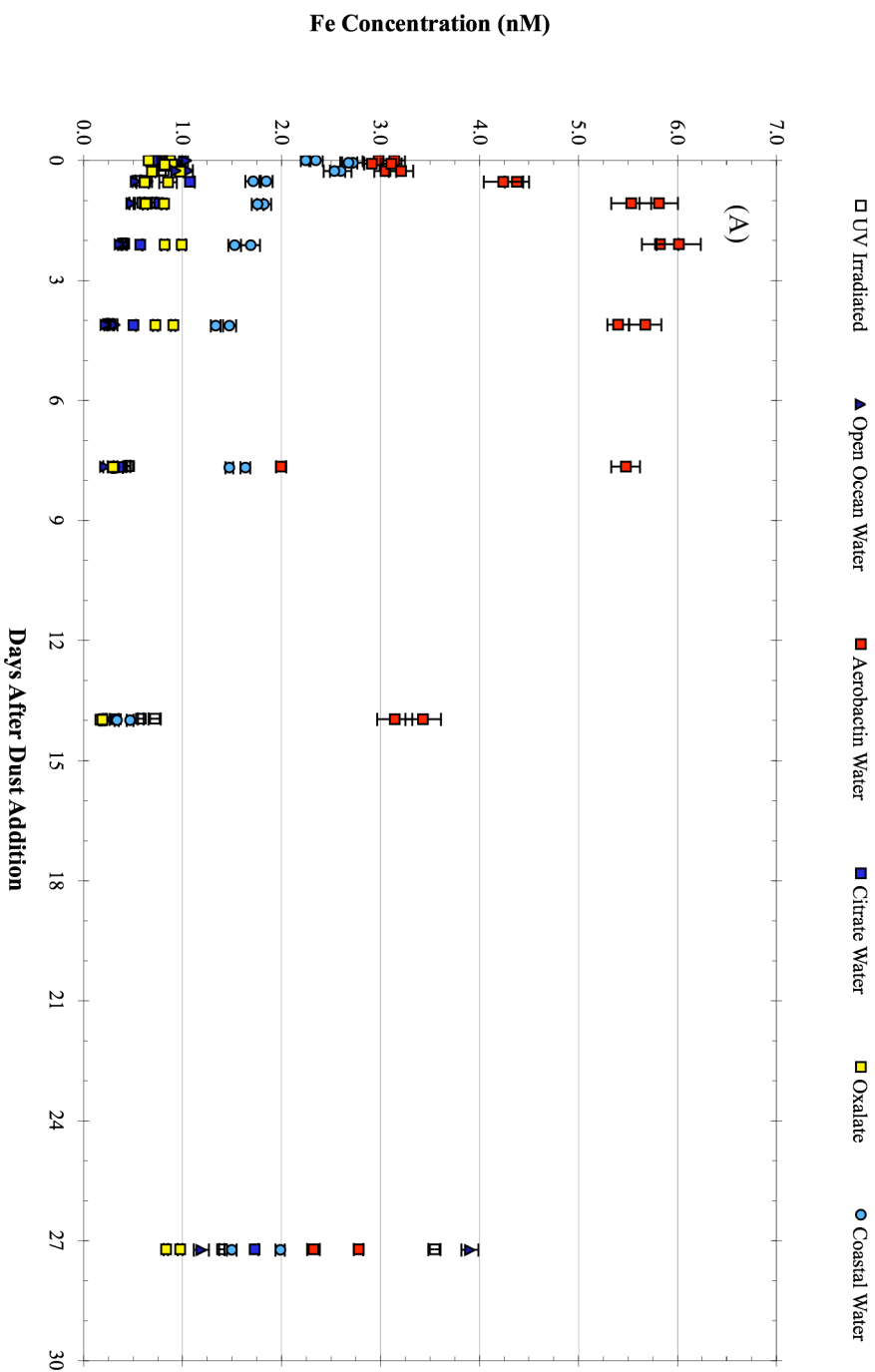


Figure 3: Fe concentrations over time in the seawater matrix experiment. Seawater samples (A) all have reductions in Fe concentration after 28 days, except the Aerobactin Water. Control samples (B) have a slow reduction in Fe concentration as Fe precipitates to the surfaces within the sample. Error bars are two  $\sigma$  of the standard error of the mean computed from the isotope dilution equation. Error bars were removed from some control samples for clarity, and are smaller than the symbols.

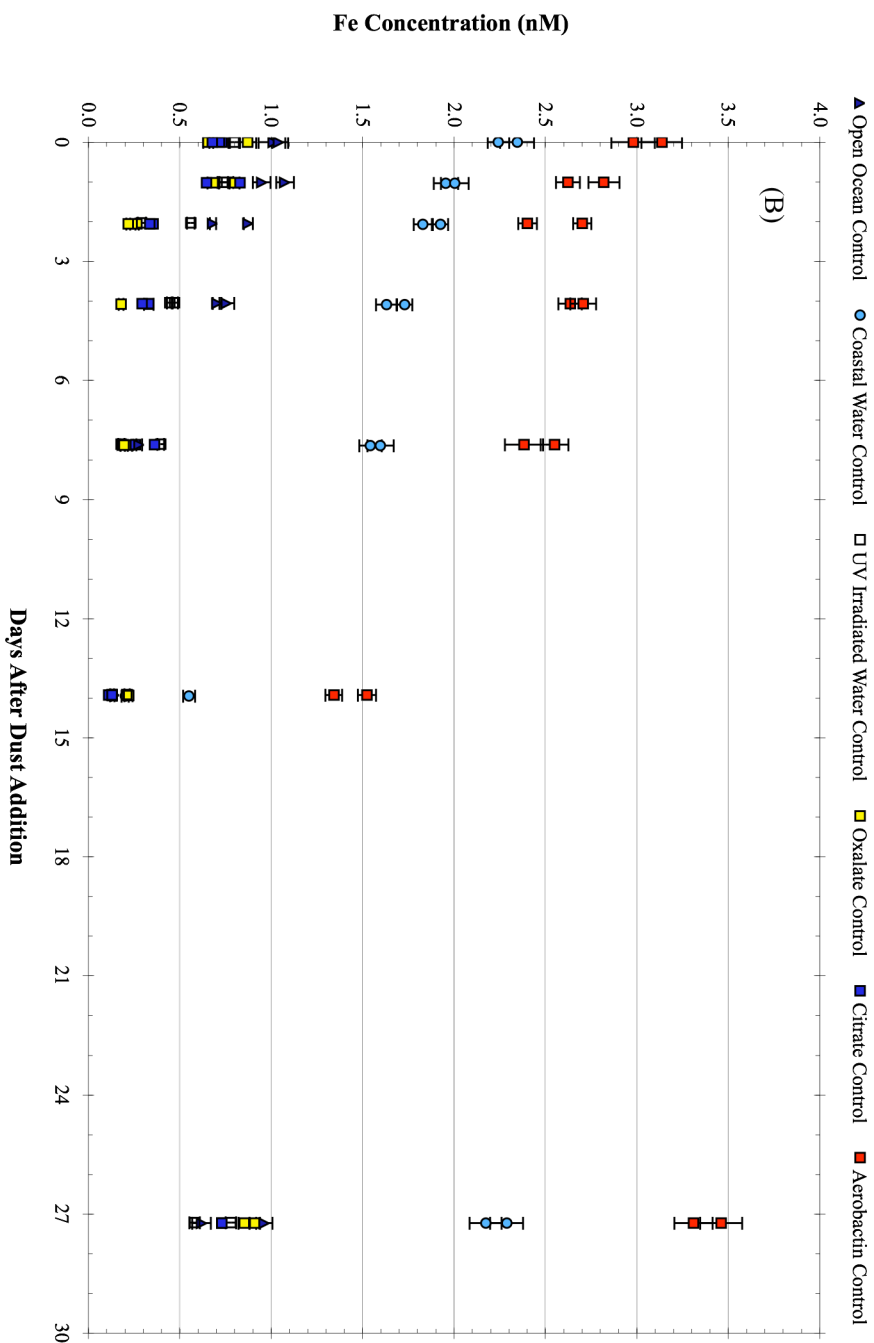


Figure 3: Fe concentrations over time in the seawater matrix experiment. Seawater samples (A) all have reductions in Fe concentration after 28 days, except the Aerobactin Water. Control samples (B) have a slow reduction in Fe concentration as Fe precipitates to the surfaces within the sample. Error bars are two  $\sigma$  of the standard error of the mean computed from the isotope dilution equation. Error bars were removed from some control samples for clarity, and are smaller than the symbols.

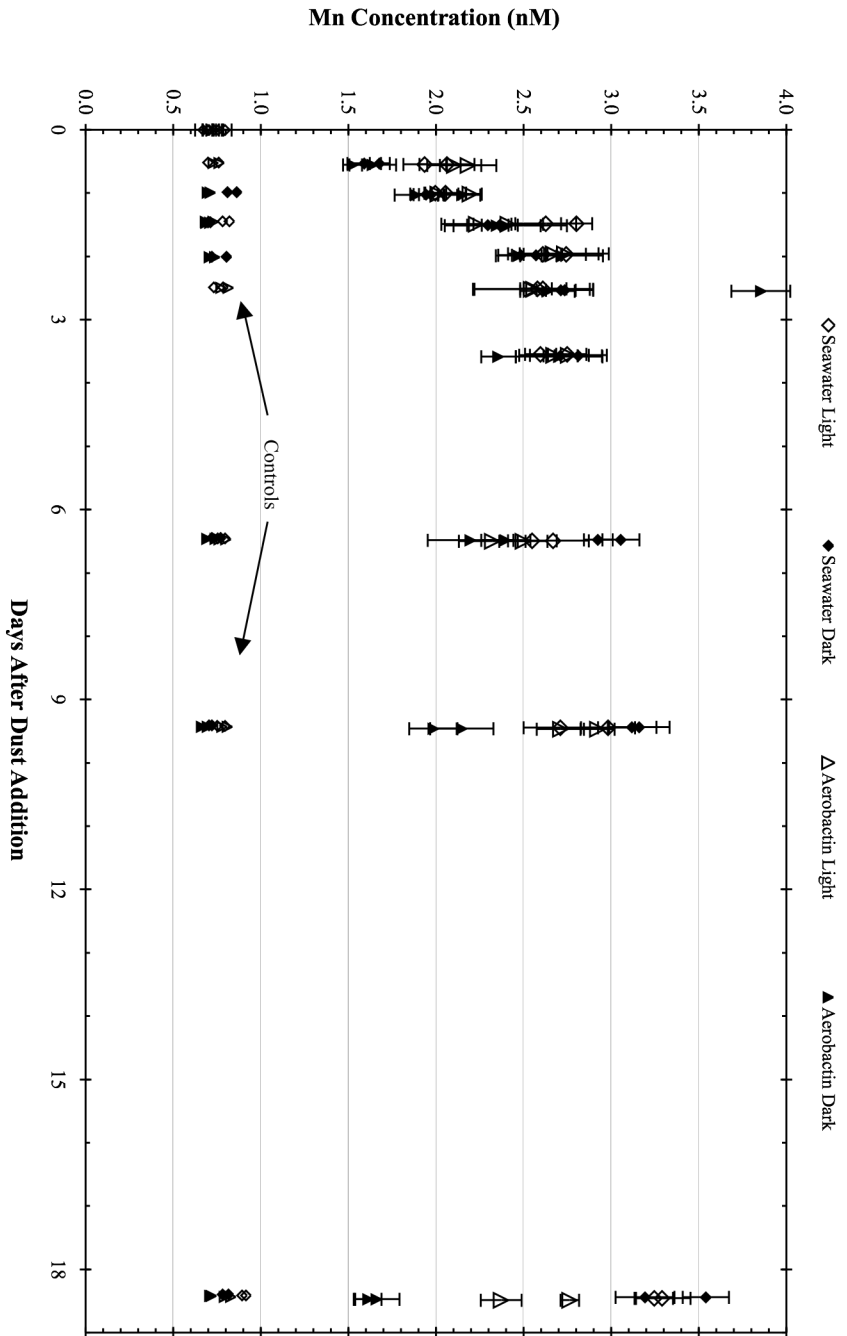


Figure 4: Mn concentrations over time for the light exposure experiment. Seawater samples and controls are shown as diamonds, Aerobactin samples and control are shown as triangles. Light exposure is denoted by the open symbols, while Dark samples are shown as closed symbols. Error bars are two  $\sigma$  of the standard error of the mean computed from the isotope dilution equation. Error bars were removed from some control samples for clarity, and are smaller than the symbols.

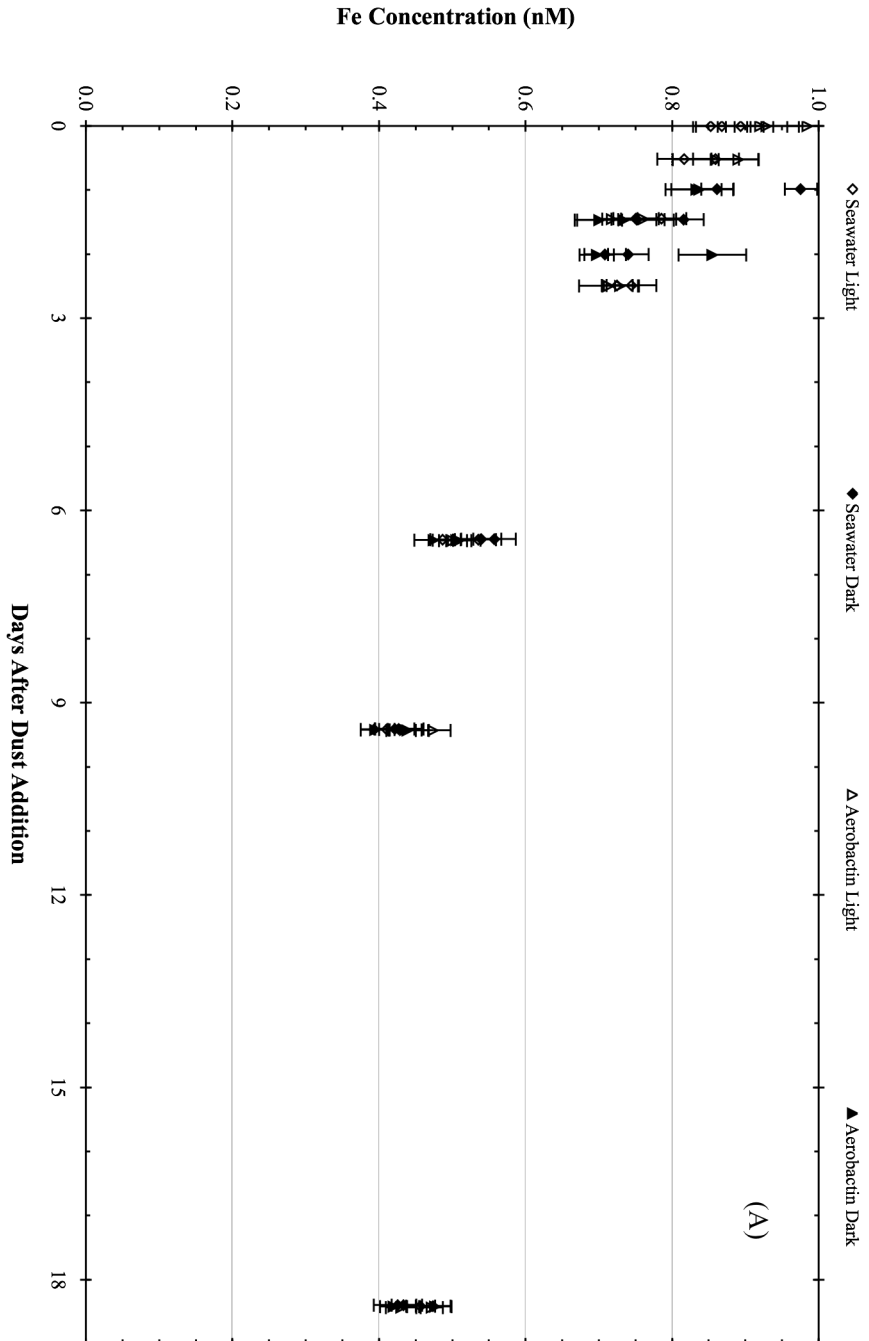


Figure 5: Fe concentration over time for light exposure experiment. Control samples (A) and have a slow reduction in Fe concentration as Fe precipitates to the surfaces within the sample. Aerobactin and Seawater samples (B) have Fe concentration increases above initial values. Error bars are two  $\sigma$  of the standard error of the mean computed from the isotope dilution equation. Error bars were removed from some control samples for clarity, and are smaller than the symbols.

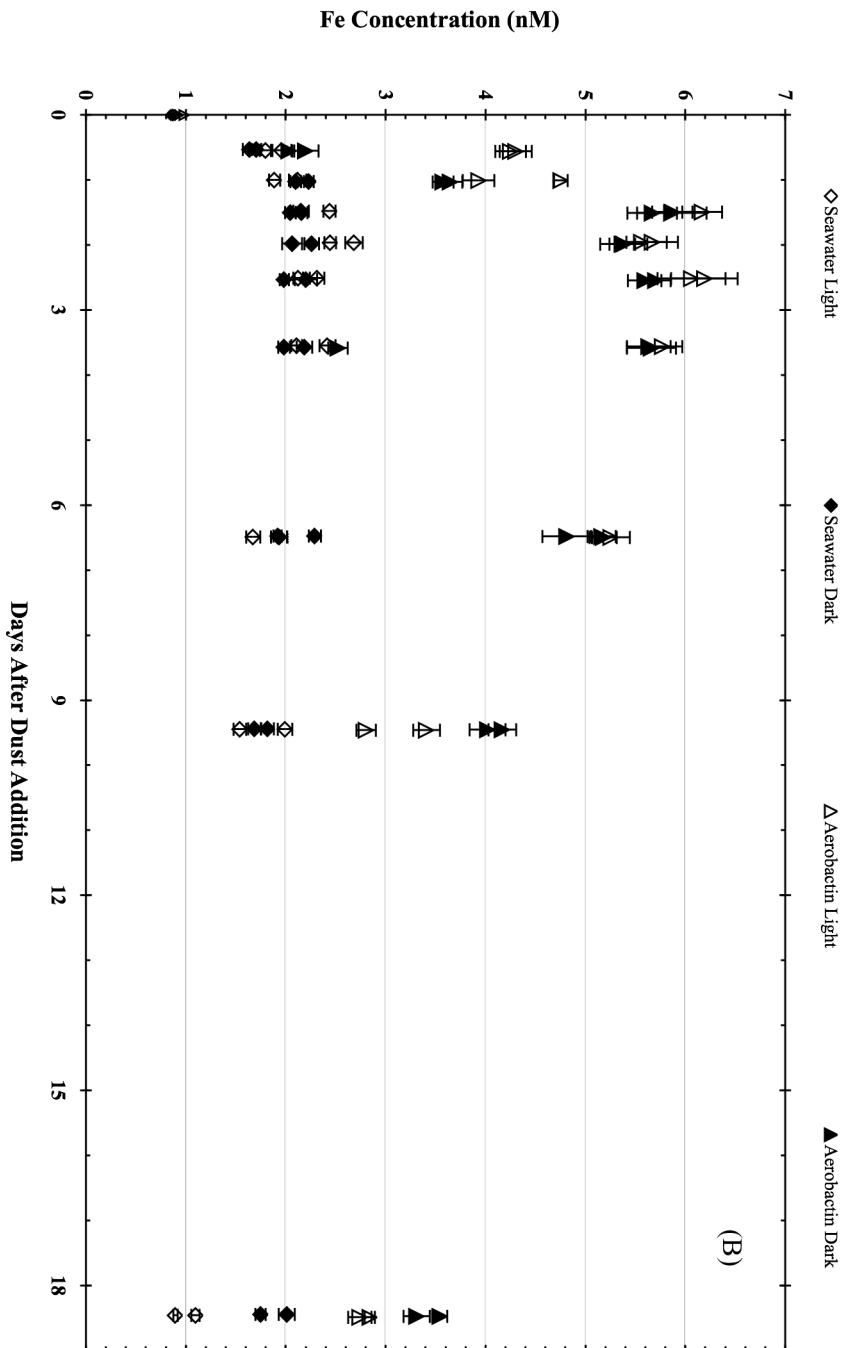


Figure 5: Fe concentration over time for light exposure experiment. Control samples (A) and have a slow reduction in Fe concentration as Fe precipitates to the surfaces within the sample. Aerobacin and Seawater samples (B) have Fe concentration increases above initial values. Error bars are two  $\sigma$  of the standard error of the mean computed from the isotope dilution equation. Error bars were removed from some control samples for clarity, and are smaller than the symbols.

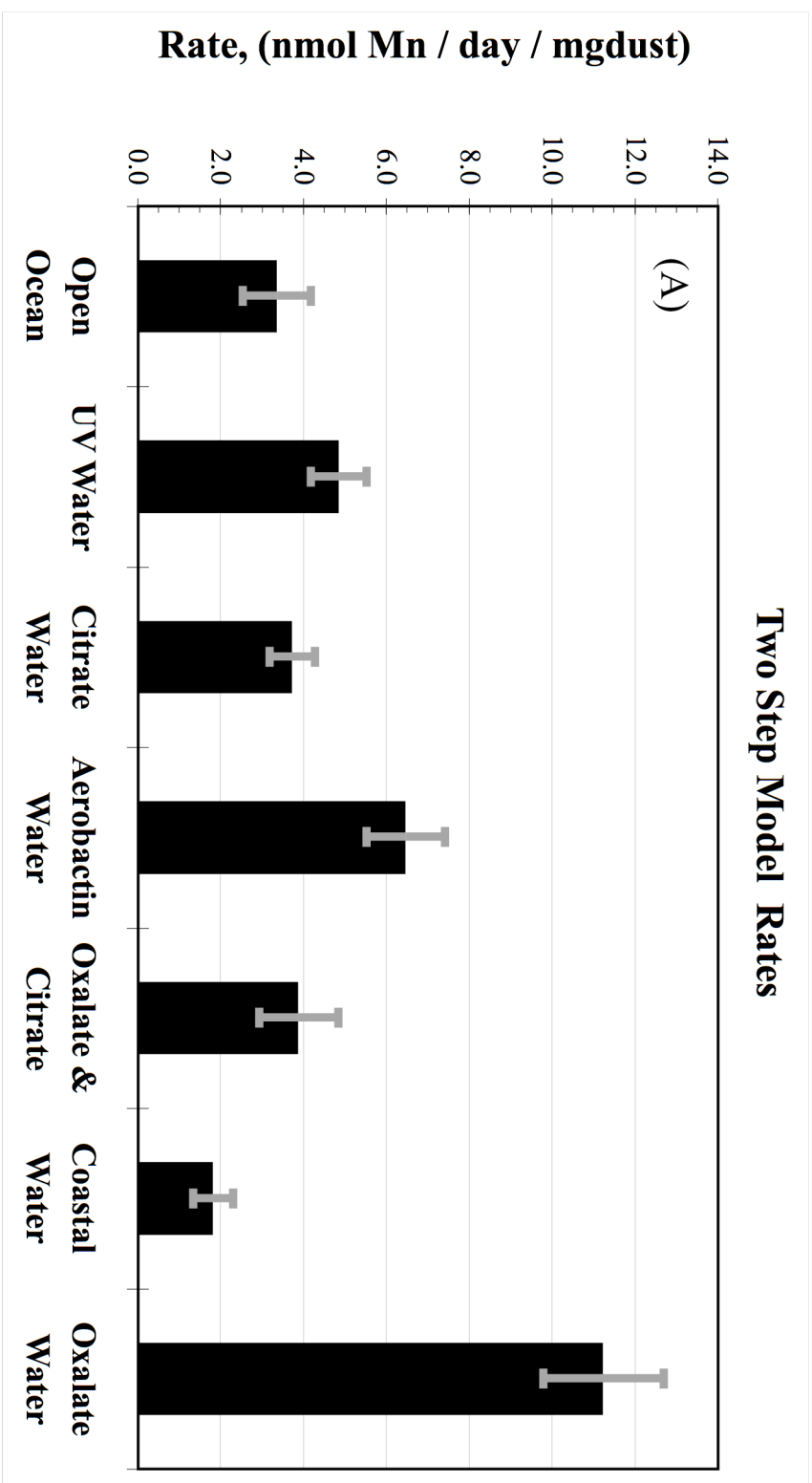


Figure 6: The calculated rates of Mn dissolution for each sample in the seawater matrix experiment (A) and light experiment (B). Oxalate promoted Mn dissolution is significantly faster than all other samples. The Coastal Water is reduced due to its large initial Mn concentration. Both Aerobactin Dark and Seawater Dark samples have diminished Mn dissolution compared to their illuminated counterpart. Error bars are determined to be 12-25% through a series of sensitivity studies on the model which varied the three independent variables.

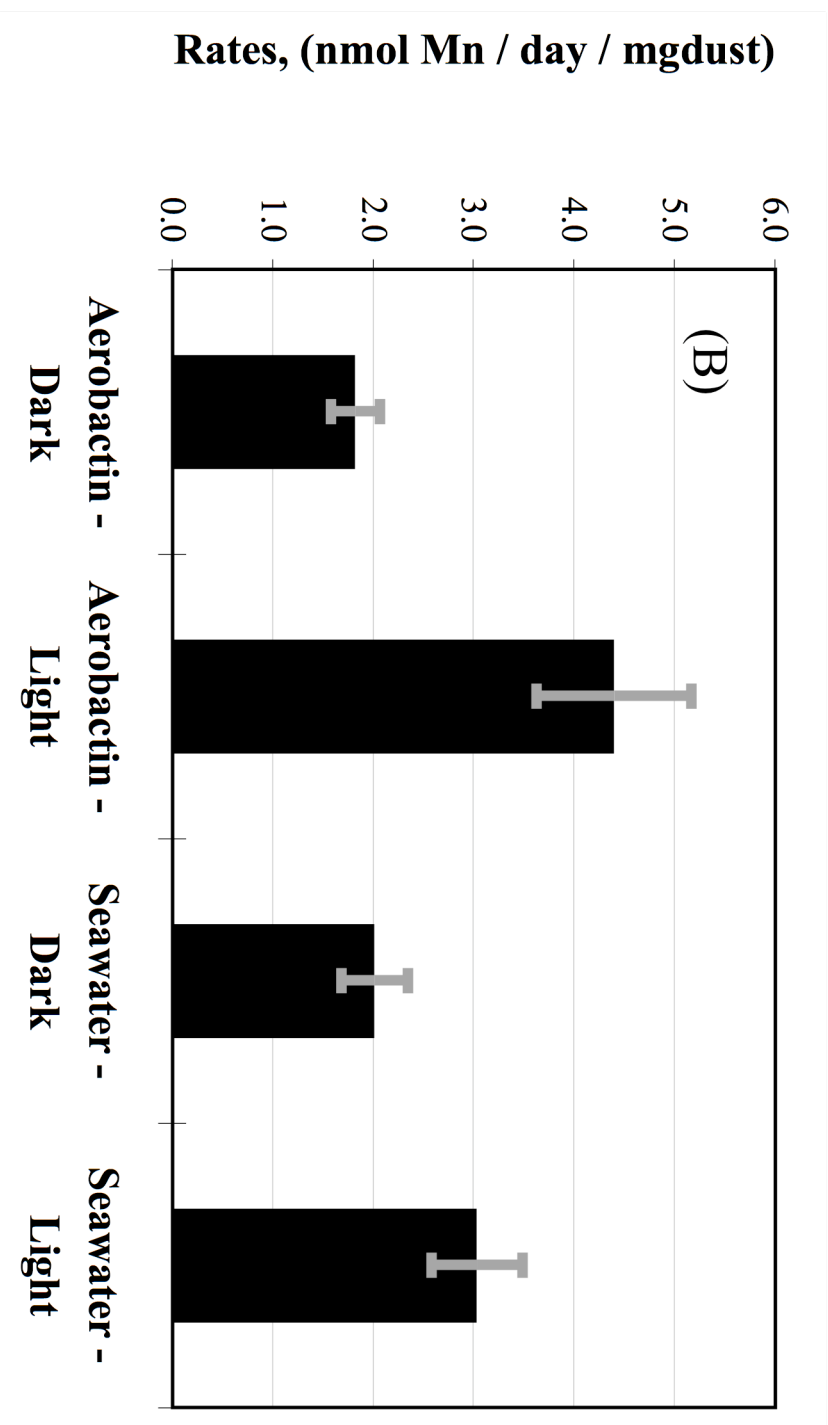


Figure 6: The calculated rates of Mn dissolution for each sample in the seawater matrix experiment (A) and light experiment (B). Oxalate promoted Mn dissolution is significantly faster than all other samples. The Coastal Water is reduced due to its large initial Mn concentration. Both Aerobactin Dark and Seawater Dark samples have diminished Mn dissolution compared to their illuminated counterpart. Error bars are determined to be 12-25% through a series of sensitivity studies on the model which varied the three independent variables.

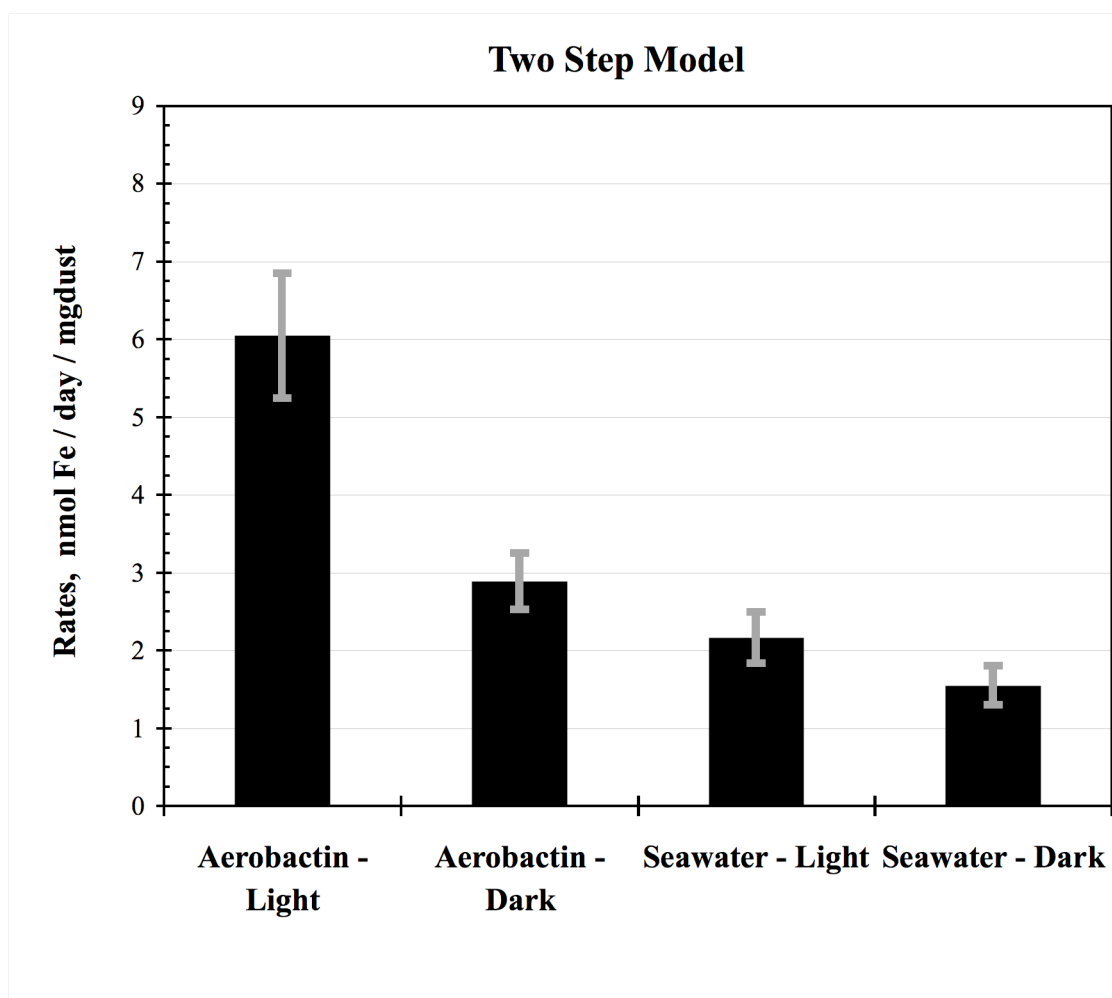
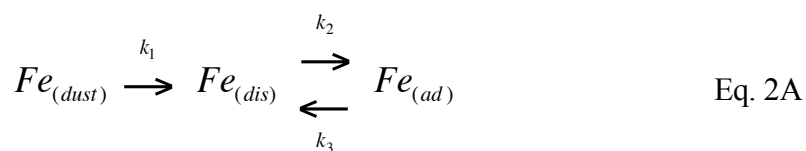
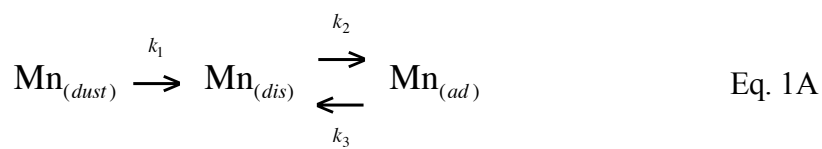


Figure 7: Calculated reaction rates for the initial dissolution of the Fe from dust using a two step reaction. The initial rate is the derivative of the equation at the point of dust addition divided by the dust concentration. Error bars are determined to be 12-25% through a series of sensitivity studies on the model which varied the three independent variables.

## APPENDIX I

The dissolution of Mn and Fe in our experiments were modeled using a two step reaction. Our model consists of an irreversible dissolution reaction, followed by an equilibrium reaction between the dissolved and adsorbed metal Eq. 1A (Mn) and 2A (Fe). The irreversible dissolution reaction is meant to model the metal coming off the dust particles, entering into the dissolved phase. Once in the dissolved phase, the metal can stay there, or adsorb onto one of many surfaces found in our experiment.



In order to calculate the dissolution rate of the metal, we need to fit the kinetic solution to the model with our data for each of the experimental samples. To do this we set up three differential equations, one for each of the metal species: metal attached to the original dust,  $M_{dust}$ ; metal in the dissolved form,  $M_{dis}$ ; and metal in the adsorbed form,  $M_{ads}$ .

$$\frac{\partial}{\partial t}[M_{dust}] = -k_1[M_{dust}] \quad \text{Eq. 3A}$$

$$\frac{\partial}{\partial t}[M_{dis}] = k_1[M_{dust}] - k_2[M_{dis}] + k_3[M_{ads}] \quad \text{Eq. 4A}$$

$$\frac{\partial}{\partial t}[M_{ads}] = k_2[M_{dis}] - k_3[M_{ads}] \quad \text{Eq. 5A}$$

To analytically solve these equations we made the following assumptions:

$M_{dust}^{t=\infty} = 0$ ,  $M_{dis}^{t=\infty} = M_{dis}^{eq}$ ,  $M_{ads}^{t=\infty} = M_{ads}^{eq}$ ,  $M_{ads}^{t=0} = 0$ . Where “t” equals time, “eq” represents equilibrium value, and  $M_{dis}^{eq}$  is assigned the average value of our data at the final sub-sample.

These assumptions then lead to the assumptions:

$M_{total}^{t=0} = M_{dust}^{t=0} + M_{dis}^{t=0}$ ,  $M_{total}(t) = M_{dust}(t) + M_{dis}(t) + M_{ads}(t)$ ,  $M_{total}^{t=\infty} = M_{dis}^{t=\infty} + M_{ads}^{t=\infty}$   
 Where  $M_{dis}^{t=0}$  is assigned the value of our data at time equals zero. Combining these assumptions we arrive at equation 6A:

$$M_{ads}(t) = M_{dust}^{t=0} - M_{dust}(t) + M_{dis}^{t=0} - M_{dis}(t) \quad \text{Eq. 6A}$$

These assumptions were used to find the analytical solution to the three differential equations:

$$M_{dust}^t = M_{dust}^{t=0} e^{(-k_1 t)} \quad \text{Eq. 7A}$$

$$M_{dis}^t = M_{dust}^{t=0} \frac{(k_1 - k_3)}{(k_2 + k_3 - k_1)} e^{-(k_1 t)} + (M_{dust}^{t=0} + M_{dis}^{t=0}) \frac{k_3}{(k_2 + k_3)} - M_{dust}^{t=0} \frac{(k_1 - k_3)}{(k_2 + k_3 - k_1)} e^{-(k_2 + k_3)t} - (M_{dust}^{t=0} + M_{dis}^{t=0}) \frac{k_3}{(k_2 + k_3)} e^{-(k_2 + k_3)t} + M_{dis}^{t=0} e^{-(k_2 + k_3)t} \quad \text{Eq. 8A}$$

Eq. 9A

$$M_{ads}^t = -M_{dust}^{t=0} \frac{k_2}{(k_2 + k_3 - k_1)} e^{-(k_1 t)} + (M_{dust}^{t=0} + M_{dis}^{t=0}) \frac{k_2}{(k_2 + k_3)} + M_{dust}^{t=0} \frac{(k_1 - k_3)}{(k_2 + k_3 - k_1)} e^{-(k_2 + k_3)t} + (M_{dust}^{t=0} + M_{dis}^{t=0}) \frac{k_3}{(k_2 + k_3)} e^{-(k_2 + k_3)t} - M_{dis}^{t=0} e^{-(k_2 + k_3)t} \quad \text{Eq. 9A}$$

and the derivative of  $M_{dis}$  at  $t = 0$ , which we use to calculate the initial dissolution rate.

$$\left. \frac{dM_{dis}}{dt} \right|_{t=0} = -M_{dust}^{t=0} \frac{k_1(k_1 - k_3)}{(k_2 + k_3 - k_1)} + M_{dust}^{t=0} \frac{(k_2 + k_3)(k_1 - k_3)}{(k_2 + k_3 - k_1)} + (M_{dust}^{t=0} + M_{dis}^{t=0}) k_3 - M_{dis}^{t=0} (k_2 + k_3) \quad \text{Eq. 10A}$$

These three solutions have five independent variables:  $M_{dust}^{t=0}$ ,  $M_{dis}^{t=0}$ ,  $k_1$ ,  $k_2$ ,  $k_3$ . To reduce the number of independent variables to three, we define:

$$K_{eq} = \frac{k_2}{k_3} = \frac{M_{ads}^{eq}}{M_{dis}^{eq}} \quad \text{Eq. 11A}$$

and by substituting in our assumptions we get

$$K_{eq} = \frac{M_{dust}^{t=0} + M_{dis}^{t=0} - M_{dis}^{eq}}{M_{dis}^{eq}} \quad \text{Eq. 12A}$$

where  $M_{dis}^{t=0}$ , and  $M_{dis}^{eq}$  are calculated from the data. Therefore  $k_3$  is defined by  $M_{dust}^{t=0}$  and  $k_2$ , and our three independent variables are  $M_{dust}^{t=0}$ ,  $k_1$ , and  $k_2$ .

To quantify the accuracy of our model fit to the data, we defined

$$\chi^2 = \frac{(M_{dis}(t) - M_{data}(t))^2}{\sigma_{data}^2(t)}, \quad \text{Eq. 13A}$$

where  $M_{dis}(t)$  and  $M_{data}(t)$  are the concentration of dissolved metal at time  $t$  for the model and the data, respectively. We used the Microsoft Excel Solver, which uses a Generalized Reduced Gradient (GRG2) nonlinear optimization algorithm, to fit the three independent variables to best fit the data by minimizing  $\chi^2$ . Multiple combinations of these independent variables are possible solutions; therefore, we optimized one variable at a time. This ensured that the solution was within realistic conditions.

For the Mn model, we began with the assumption that  $Mn_{dust}^{t=0}$  is the same for every experiment. We set  $M_{dust}^{t=0}$  to 4 nM (the average increase in [Mn] for all experiments) and

solved for  $k_1$  and  $k_2$  by minimizing  $\sum_t^{t=eq} \chi^2$ . We fit  $k_1$  and  $k_2$  for every sample in both

experiments then repeated this process for  $Mn_{dust}^{t=0} = 4.25 - 15$  nM. We plot  $\sum_t^{t=eq} \chi^2$  for

Oxalate Water and total  $\sum_t^{t=eq} \chi^2$  for all samples in figure 1A, and show the  $Mn_{dust}^{t=0}$  at the

minimum  $\sum_t^{t=eq} \chi^2$  for each experiment in Table A-1. The  $Mn_{dust}^{t=0}$  for all samples has an

average of 35% of the total Mn within the added dust. (Guieu *et al.*, 1994) also found 35% dissolution of Mn from aerosol particles in seawater. Therefore, we set  $Mn_{dust}^{t=0}$  to 35% of

the total Mn of the dust added to each sample. The dust added to each sample was not the same; therefore,  $Mn_{dust}^{t=0}$  is different in each sample. With  $Mn_{dust}^{t=0}$  set at 35%, we re-solved

the model for  $k_1$  and  $k_2$ , and calculated  $\frac{d}{dt} Mn_{dis}^{t=0}$ . The initial rate of Mn dissolutions is

$\frac{d}{dt} Mn_{dis}^{t=0}$  divided by the mass of dust for each sample.

Sensitivity of the rate to  $Mn_{dust}^{t=0}$ ,  $k_1$ , and  $k_2$  was determined by fixing two of the three independent variables to their “best fit” value, and varying the third  $\pm 20\%$ . We tracked the change in  $\frac{d}{dt}Mn_{dis}^{t=0}$  with the change in  $k_1$  or  $k_2$ , and calculated the mean and standard deviation of  $\frac{d}{dt}Mn_{dis}^{t=0}$  over the change. To calculate the sensitivity with respect to  $Mn_{dust}^{t=0}$ , we “re-fit” the model after each variation to  $Mn_{dust}^{t=0}$ . The sensitivity of  $\frac{d}{dt}Mn_{dis}^{t=0}$  to the variable of interest was defined as the standard deviation of the mean  $\frac{d}{dt}Mn_{dis}^{t=0}$  divided by the mean. The sensitivity of dissolution rate to the independent variables is listed in Table A-2. Overall, the samples are most sensitive to  $k_1$ , which is the rate constant of the dissolution step, and are insensitive to changes in  $k_2$ , because  $k_2$  is important only after significant quantities of dissolved Mn accumulate. Only the Coastal Water sample has any significant quantity of dissolved Mn at time zero, and the Coastal Water is the only sample which is sensitive to changes in  $k_2$ . Sensitivity to the quantity of soluble Mn in the dust varies from 0.33% in the Dark Aerobactin sample to 8.3% in the Citrate sample.

For the Fe reaction we used the control samples to constrain  $k_2$ , and then fit the other independent variables to the data using the two step reaction model outlined above. In our model for the control samples,  $Fe_{dis}^t$  was in a reversible reaction with  $Fe_{ads}^t$ , without the irreversible dissolution step. We only fit the Fe data in the light experiment.

We set up the differential equations

$$\frac{\partial}{\partial t}[Fe_{dis}] = -k_2[Fe_{dis}] + k_3[Fe_{ads}] \quad , \quad \text{Eq. 14A}$$

$$\frac{\partial}{\partial t}[Fe_{ads}] = k_2[Fe_{dis}] - k_3[Fe_{ads}] \quad , \quad \text{Eq. 15A}$$

and solved for the dissolved species

$$Fe_{dis}^t = (Fe_{dis}^{t=0} - Fe_{dis}^{t=eq})e^{-ct} + Fe_{dis}^{t=eq} \quad . \quad \text{Eq. 16A}$$

We solved for  $\alpha$  in each of the four controls, and calculated  $k_3$  for each of the corresponding dust samples using the equation  $k_3 = \frac{\alpha}{(K_{eq} + 1)}$ , where  $\alpha = k_2 + k_3$ . The variable  $k_2$  was constrained by  $k_3$  and the equilibrium constant using Eq. 13A. We then used the Excel solver to solve the best fit for  $Fe_{dust}^{t=0}$  and  $k_1$ .

The best fit values for  $Fe_{dust}^{t=0}$  in the two aerobactin samples (light and dark) and the two natural seawaters (light and dark) were similar to each other. Therefore, we chose to further constrain the Fe dissolution model by forcing both aerobactin samples and both seawater samples to have equivalent  $Fe_{dust}^{t=0}$  to each other. Similar to the Mn case, we chose the best  $Fe_{dust}^{t=0}$  for each water type by varying  $Fe_{dust}^{t=0} \pm 50\%$  while monitoring  $\sum_t^{t=eq} \chi^2$ . The

$Fe_{dust}^{t=0}$  value with the minimum  $\sum_{Light}^{Dark} \sum_t \chi^2$  was chosen as the  $Fe_{dust}^{t=0}$  value for each water type. We then re-solved the model for the best fit in  $k_1$  to the data.

Sensitivity of our model to variations in our three independent variables was measured in an identical manner as the Mn model. We set two independent variables to their best fit values and varied the third. Sensitivity to  $k_1$  or  $k_2$  was determined by changing the constants  $\pm 20\%$  and monitoring the change in  $\frac{d}{dt} Fe_{dis}^{t=0}$ . The sensitivity of the derivative to changes in  $Fe_{dust}^{t=0}$  was determined by varying  $Fe_{dust}^{t=0} \pm 20\%$  and then re-solving for the best fit for  $k_1$  and  $k_2$ . In all cases, the sensitivity of our model to the independent variables was defined as the standard deviation of the mean  $\frac{d}{dt} Fe_{dis}^{t=0}$  divided by the mean. The sensitivities are reported in Table A-3. As in the Mn model, the derivative in  $Fe_{dis}$  is sensitive to changes in  $k_1$  and insensitive to  $k_2$ , with mixed sensitivity to the available Fe in the dust.

## APPENDIX TABLES AND FIGURES

<b>Sample</b>	<b><math>Mn_{dust}^{\prime-0}</math> at minimum, nM</b>	<b>Percentage of <math>Mn_{total}</math></b>
Open Ocean	5.25	33.2%
Coastal Water	> 15	-
UV Water	5.50	35.1%
Citrate Water	6.00	37.7%
Aerobactin Water	5.00	31.5%
Oxalate & Citrate Water	4.50	38.9%
Oxalate Water	5.25	33.2%
Aerobactin – Light Water	5.25	35.3%
Aerobactin – Dark Water	>15	-
Seawater – Light Water	5.50	36.0%
Seawater – Dark Water	5.50	36.0%
Average	5.31	35.2%

Table A-1: The quantity of available Mn from the dust according to the Mn two step model. Each value given is the value of  $Mn_{dust}$  which resulted in the minimum  $\chi^2$  values for the overall fit to the data. The Coastal Water and Aerobactin-Dark samples never reached a minimum.

<b>Sample</b>	<b>Mean</b> $\frac{d}{dt} Mn_{dis}^{t=0}$	<b>Sensitivity to</b> $Mn_{dust}^{t=0}$	<b>Sensitivity to</b> $k_1$	<b>Sensitivity to</b> $k_2$
Open Ocean	3.89	4.1%	13.6%	1.6%
Coastal Water	2.11	0.51%	23.9%	11.9%
UV Water	5.56	7.0%	12.0%	0.01%
Citrate Water	4.35	8.3%	12.1%	0.12%
Aerobactin Water	7.53	7.1%	12.8%	0.82%
Oxalate & Citrate Water	3.29	5.9%	13.0%	1.03%
Oxalate Water	13.04	4.7%	12.0%	0.03%
Aerobactin – Light Water	4.79	5.1%	16.2%	4.17%
Aerobactin – Dark Water	1.99	0.33%	13.4%	1.37%
Seawater – Light Water	3.39	2.0%	14.6%	2.59%
Seawater – Dark Water	2.25	3.5%	15.6%	3.61%

Table A-2: Sensitivity study for the Mn two step model. Each independent variable was changed  $\pm 20\%$  while monitoring the derivative in  $Mn_{dis}$ . The sensitivity of the derivative to the variable was defined as the standard deviation in mean of the derivative divided by the mean.

<b>Sample</b>	<b>Average</b> $\frac{d}{dt} Fe_{dis}^{t=0}$	<b>Sensitivity to</b> $Fe_{dust}^{t=0}$	<b>Sensitivity to</b> $k_1$	<b>Sensitivity to</b> $k_2$
Aerobactin – Light Water	6.96	0.66%	12.2%	0.21%
Aerobactin – Dark Water	3.52	5.3%	12.5%	0.51%
Seawater – Light Water	2.63	10.3%	12.6%	0.59%
Seawater – Dark Water	1.94	8.5%	12.4%	0.45%

Table A-3: Sensitivity Study for the Fe two step model. Each independent variable was changed  $\pm 20\%$  while monitoring the derivative in  $Mn_{dis}$ . The sensitivity of the derivative to the variable was defined as the standard deviation in mean of the derivative divided by the mean.

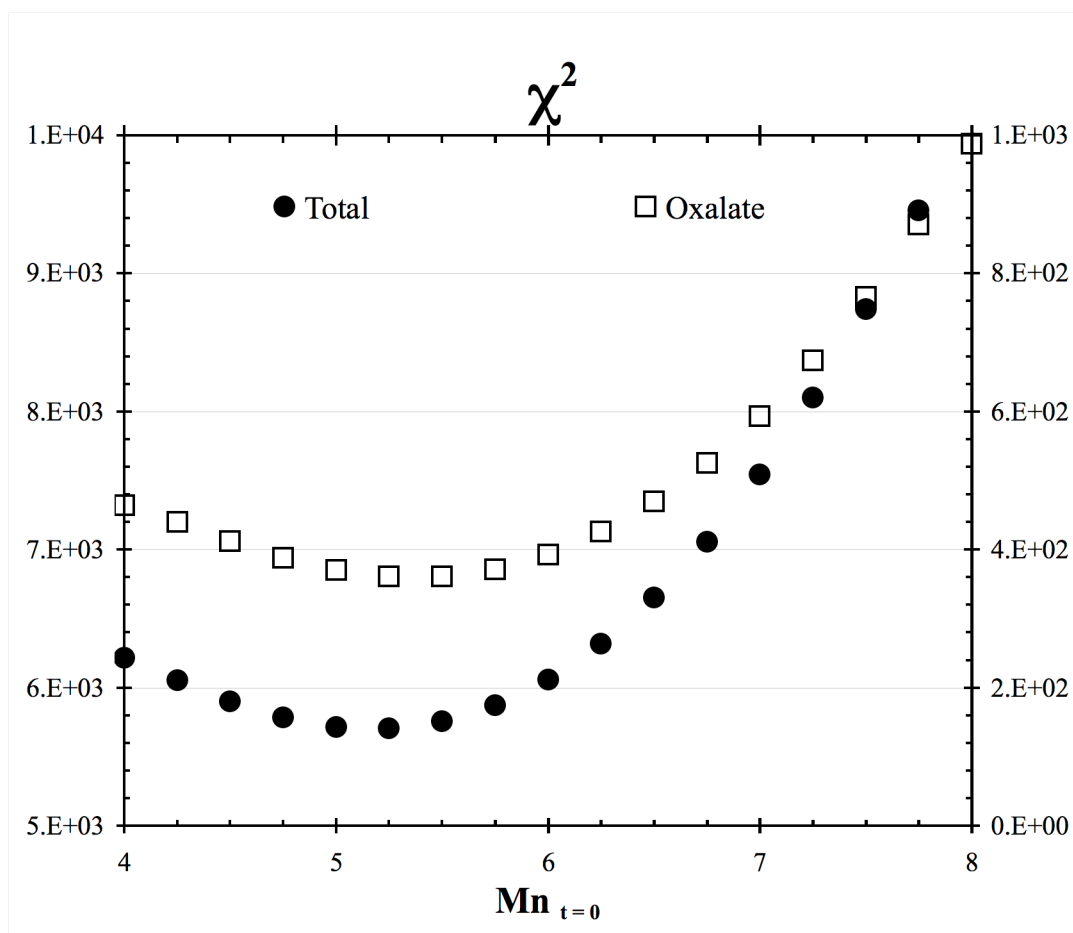


Figure 1A:  $\chi^2$  (eq. 13A) is a measure of the accuracy of the model fit to the data. To select the appropriate constants for our model, we minimized  $\chi^2$  for each water sample. Here the sum of the  $\chi^2$  is plotted against the change in total Mn available from the dust,  $Mn_{dust}$ , for both Oxalate Water and the total of all water samples. A value of 5.25 nM was selected as the best fit to the data for this circumstance.

## BIBLIOGRAPHY

- Banerjee, D. and Nesbitt, H.W., 1999. XPS study of reductive dissolution of birnessite by oxalate: Rates and mechanistic aspects of dissolution and redox processes. *Geochimica Et Cosmochimica Acta*, 63(19-20): 3025-3038.
- Barbeau, K., 2006. Photochemistry of organic iron(III) complexing ligands in oceanic systems. *Photochemistry and Photobiology*, 82(6): 1505-1516.
- Barbeau, K., Rue, E.L., Bruland, K.W. and Butler, A., 2001. Photochemical cycling of iron in the surface ocean mediated by microbial iron(III)-binding ligands. *Nature*, 413: 409-413.
- Barbeau, K., Rue, E.L., Trick, C.G., Bruland, K.T. and Butler, A., 2003. Photochemical reactivity of siderophores produced by marine heterotrophic bacteria and cyanobacteria based on characteristic Fe(III) binding groups. *Limnology and Oceanography*, 48(3): 1069-1078.
- Barbeau, K., Zhang, G.P., Live, D.H. and Butler, A., 2002. Petrobactin, a photoreactive siderophore produced by the oil-degrading marine bacterium *Marinobacter hydrocarbonoclasticus*. *Journal of the American Chemical Society*, 124(3): 378-379.
- Bonnet, S. and Guieu, C., 2004. Dissolution of atmospheric iron in seawater. *Geophysical Research Letters*, 31(3).
- Borer, P.M., Sulzberger, B., Reichard, P. and Kraemer, S.M., 2005. Effect of siderophores on the light-induced dissolution of colloidal iron(III) (hydr)oxides. *Marine Chemistry*, 93(2-4): 179-193.
- Boukhalfa, H. and Crumbliss, A.L., 2002. Chemical aspects of siderophore mediated iron transport. *Biometals*, 15(4): 325-339.
- Braun, V., 2003. Iron uptake by *Escherichia coli*. *Frontiers in Bioscience*, 8: S1409-S1421.
- Buck, C.S., Landing, W.M., Resing, J.A. and Lebon, G.T., 2006. Aerosol iron and aluminum solubility in the northwest Pacific Ocean: Results from the 2002 IOC cruise. *Geochemistry Geophysics Geosystems*, 7.
- Buck, K.N., Lohan, M.C., Berger, C.J.M. and Bruland, K.W., 2007. Dissolved iron speciation in two distinct river plumes and an estuary: Implications for riverine iron supply. *Limnology and Oceanography*, 52(2): 843-855.
- Cheah, S.F., Kraemer, S.M., Cervini-Silva, J. and Sposito, G., 2003. Steady-state dissolution kinetics of goethite in the presence of desferrioxamine B and oxalate ligands: implications for the microbial acquisition of iron. *Chemical Geology*, 198(1-2): 63-75.
- Cocozza, C. et al., 2002. Temperature dependence of goethite dissolution promoted by trihydroxamate siderophores. *Geochimica Et Cosmochimica Acta*, 66(3): 431-438.

- Donat, J.R. and Bruland, K.W., 1988. Direct Determination of Dissolved Cobalt and Nickel in Seawater by Differential Pulse Cathodic Stripping Voltammetry Preceded by Adsorptive Collection of Cyclohexane-1,2-Dione Dioxime Complexes. *Analytical Chemistry*, 60(3): 240-244.
- Duce, R.A. and Tindale, N.W., 1991. Atmospheric transport of iron and its deposition in the ocean. *Limnology and Oceanography*, 36(8): 1715-1726.
- Duckworth, O.W. and Martin, S.T., 2001. Surface complexation and dissolution of hematite by C-1-C-6 dicarboxylic acids at pH=5.0. *Geochimica Et Cosmochimica Acta*, 65(23): 4289-4301.
- Erel, Y., Pehkonen, S.O. and Hoffmann, M.R., 1993. Redox Chemistry of Iron in Fog and Stratus Clouds. *Journal of Geophysical Research-Atmospheres*, 98(D10): 18423-18434.
- Furrer, G. and Stumm, W., 1986. The Coordination Chemistry of Weathering .1. Dissolution Kinetics of Delta-Al<sub>2</sub>O<sub>3</sub> and BeO<sub>2</sub>. *Geochimica Et Cosmochimica Acta*, 50(9): 1847-1860.
- Guieu, C., Duce, R. and Arimoto, R., 1994. Dissolved Input of Manganese to the Ocean - Aerosol Source. *Journal of Geophysical Research-Atmospheres*, 99(D9): 18789-18800.
- Harris, W.R., Carrano, C.J. and Raymond, K.N., 1979. Coordination Chemistry of Microbial Iron Transport Compounds .16. Isolation, Characterization, and Formation-Constants of Ferric Aerobactin. *Journal of the American Chemical Society*, 101(10): 2722-2727.
- Haygood, M.G., Holt, P.D. and Butler, A., 1993. Aerobactin Production by a Planktonic Marine *Vibrio* Sp. *Limnology and Oceanography*, 38(5): 1091-1097.
- Hersman, L., Lloyd, T. and Sposito, G., 1995. Siderophore-Promoted Dissolution of Hematite. *Geochimica Et Cosmochimica Acta*, 59(16): 3327-3330.
- Holmen, B.A. and Casey, W.H., 1996. Hydroxamate ligands, surface chemistry, and the mechanism of ligand-promoted dissolution of goethite [ $\alpha$ -FeOOH(s)]. *Geochimica Et Cosmochimica Acta*, 60(22): 4403-4416.
- Johansen, A.M., Siefert, R.L. and Hoffmann, M.R., 2000. Chemical composition of aerosols collected over the tropical North Atlantic Ocean. *Journal of Geophysical Research-Atmospheres*, 105(D12): 15277-15312.
- Johnson, K.S. et al., 2007. Developing Standards for Dissolved Iron in Seawater. *EOS*, 88(11): 131-132.
- Jun, Y.S. and Martin, S.T., 2003. Microscopic observations of reductive manganese dissolution under oxic conditions. *Environmental Science & Technology*, 37(11): 2363-2370.
- Klewicki, J.K. and Morgan, J.J., 1998. Kinetic behavior of Mn(III) complexes of pyrophosphate, EDTA, and citrate. *Environmental Science & Technology*, 32(19): 2916-2922.

- Klewicki, J.K. and Morgan, J.J., 1999. Dissolution of beta-MnOOH particles by ligands: Pyrophosphate, ethylenediaminetetraacetate, and citrate. *Geochimica Et Cosmochimica Acta*, 63(19-20): 3017-3024.
- Kraemer, S.M., 2004. Iron oxide dissolution and solubility in the presence of siderophores. *Aquatic Sciences*, 66(1): 3-18.
- Küpper, F.C., Carrano, C.J., Kuhn, J.U. and Butler, A., 2006. Photoreactivity of iron(III) - Aerobactin: Photoproduct structure and iron(III) coordination. *Inorganic Chemistry*, 45(15): 6028-6033.
- Macrellis, H.M., Trick, C.G., Rue, E.L., Smith, G. and Bruland, K.W., 2001. Collection and detection of natural iron-binding ligands from seawater. *Marine Chemistry*, 76(3): 175-187.
- Mendez, J.M., Guieu, C. and Adkins, J.F., in review. Atmospheric input of Manganese and Iron to the ocean: Sea water dissolution experiments with Saharan and North American dusts. *Marine Chemistry*: (in review).
- Morel, F.M.M. and Hering, J.G., 1993. *Principles and Applications of Aquatic Chemistry*. John Wiley & Sons, Inc., New York, 588 pp.
- Neilands, J.B., 1995. Siderophores - Structure and Function of Microbial Iron Transport Compounds. *Journal of Biological Chemistry*, 270(45): 26723-26726.
- Pehkonen, S.O., Siefert, R., Erel, Y., Webb, S. and Hoffmann, M.R., 1993. Photoreduction of Iron Oxyhydroxides in the Presence of Important Atmospheric Organic-Compounds. *Environmental Science & Technology*, 27(10): 2056-2062.
- Raymond, K.N. and Carrano, C.J., 1979. Coordination Chemistry and Microbial Iron Transport. *Accounts of Chemical Research*, 12(5): 183-190.
- Rose, A.L. and Waite, T.D., 2002. Kinetic model for Fe(II) oxidation in seawater in the absence and presence of natural organic matter. *Environmental Science & Technology*, 36(3): 433-444.
- Rue, E. and Bruland, K., 2001. Domoic acid binds iron and copper: a possible role for the toxin produced by the marine diatom *Pseudo-nitzschia*. *Marine Chemistry*, 76(1-2): 127-134.
- Rue, E.L. and Bruland, K.W., 1995. Complexation of Iron(III) by Natural Organic-Ligands in the Central North Pacific as Determined by a New Competitive Ligand Equilibration Adsorptive Cathodic Stripping Voltammetric Method. *Marine Chemistry*, 50(1-4): 117-138.
- Siefert, R.L., Johansen, A.M., Hoffmann, M.R. and Pehkonen, S.O., 1998. Measurements of trace metal (Fe, Cu, Mn, Cr) oxidation states in fog and stratus clouds. *Journal of the Air & Waste Management Association*, 48(2): 128-143.
- Siefert, C. and Sulzberger, B., 1991. Light-Induced Dissolution of Hematite in the Presence of Oxalate - a Case-Study. *Langmuir*, 7(8): 1627-1634.
- Smith, R.M., Martell, A.E. and Motekaitis, R.J., 2004. *NIST Critically Selected Stability Constants of Metal Complexes Database*. National Institute of Standards and Technology.

- Stone, A.T., 1987. Microbial Metabolites and the Reductive Dissolution of Manganese Oxides - Oxalate and Pyruvate. *Geochimica Et Cosmochimica Acta*, 51(4): 919-925.
- Stone, A.T. and Morgan, J.J., 1984. Reduction and Dissolution of Manganese(II) and Manganese(IV) Oxides by Organics .2. Survey of the Reactivity of Organics. *Environmental Science & Technology*, 18(8): 617-624.
- Stumm, W. and Morgan, J.J., 1996. *Aquatic Chemistry*. Wiley-Interscience, New York, 1022 pp.
- Sunda, W.G., Huntsman, S.A. and Harvey, G.R., 1983. Photoreduction of manganese oxides in seawater and its geochemical and biological implications. *Nature*, 301: 234-236.
- Turner, D.R. and Hunter, K.A. (Editors), 2001. *The biogeochemistry of iron in seawater*. IUPAC series on analytical and physical chemistry of environmental systems ; v. 7. J. Wiley, New York.
- Voelker, B.M., Morel, F.M.M. and Sulzberger, B., 1997. Iron redox cycling in surface waters: Effects of humic substances and light. *Environmental Science & Technology*, 31(4): 1004-1011.
- von Langen, P.J., Johnson, K.S., Coale, K.H. and Elrod, V.A., 1997. Oxidation kinetics of manganese (II) in seawater at nanomolar concentrations. *Geochimica Et Cosmochimica Acta*, 61(23): 4945-4954.
- Waite, T.D. and Morel, F.M.M., 1984. Photoreductive Dissolution of Colloidal Iron-Oxide - Effect of Citrate. *Journal of Colloid and Interface Science*, 102(1): 121-137.
- Wang, Y. and Stone, A.T., 2006. Reaction of Mn-III, Mn-IV (hydr)oxides with oxalic acid, glyoxylic acid, phosphonoformic acid, and structurally-related organic compounds. *Geochimica Et Cosmochimica Acta*, 70(17): 4477-4490.
- Wedepohl, K.H., 1995. The Composition of the Continental-Crust. *Geochimica Et Cosmochimica Acta*, 59(7): 1217-1232.
- Witter, A.E., Hutchins, D.A., Butler, A. and Luther, G.W., 2000. Determination of conditional stability constants and kinetic constants for strong model Fe-binding ligands in seawater. *Marine Chemistry*, 69(1-2): 1-17.
- Wu, J. and Boyle, E.A., 1998. Determination of iron in seawater by high-resolution isotope dilution inductively coupled plasma mass spectrometry after  $Mg(OH)_2$  coprecipitation. *Analytica Chimica Acta*, 367: 183-191.
- Xyla, A.G. et al., 1992. Reductive Dissolution of Manganese(II,IV) (Hydr)Oxides by Oxalate - the Effect of Ph and Light. *Langmuir*, 8(1): 95-103.
- Yoshida, T., 2002. Dissolution of iron hydroxides by marine bacterial siderophore. *Chemical geology*, 184(1-2): 1-9.
- Zinder, B., Furrer, G. and Stumm, W., 1986. The Coordination Chemistry of Weathering .2. Dissolution of Fe(III) Oxides. *Geochimica Et Cosmochimica Acta*, 50(9): 1861-1869.